Modeling Deformation-Induced Fluid Flow in Cortical Bone's Canalicular–Lacunar System

S. Gururaja,[1] H. J. Kim,[1] C. C. Swan,[1] R. A. Brand,[2] and R. S. Lakes[3]

[1]Department of Civil and Environmental Engineering, Center for Computer-Aided Design (CCAD),
University of Iowa, Iowa City, IA, U.S.A.; [2]Clinical Orthopaedics and Related Research, Philadelphia,
PA, U.S.A.; and [3]Engineering Physics, University of Wisconsin, Madison, WI, U.S.A.

Abstract—To explore the potential role that load-induced fluid flow plays as a mechano–transduction mechanism in bone adaptation, a lacunar–canalicular scale bone poroelasticity model is developed and implemented. The model uses micromechanics to homogenize the pericanalicular bone matrix, a system of straight circular cylinders in the bone matrix through which bone fluids can flow, as a locally anisotropic poroelastic medium. In this work, a simplified two-dimensional model of a periodic array of lacunae and their surrounding systems of canaliculi is used to quantify local fluid flow characteristics in the vicinity of a single lacuna. When the cortical bone model is loaded, microscale stress, and strain concentrations occur in the vicinity of individual lacunae and give rise to microscale spatial variations in the pore fluid pressure field. Furthermore, loading of the bone matrix containing canaliculi generates fluid pressures in the contained fluids. Consequently, loading of cortical bone induces fluid flow in the canaliculi and exchange of fluid between canaliculi and lacunae. For realistic bone morphology parameters, and a range of loading frequencies, fluid pressures and fluid–solid drag forces in the canalicular bone are computed and the associated energy dissipation in the models compared to that measured in physical *in vitro* experiments on human cortical bone. The proposed model indicates that deformation-induced fluid pressures in the lacunar–canalicular system have relaxation times on the order of milliseconds as opposed to the much shorter times (hundredths of milliseconds) associated with deformation-induced pressures in the Haversian system.

Keywords—Poroelasticity, Micromechanics, Multiscale modeling, Mechanotransduction, Bone adaptation, Osteocyte, Lacuna, Canaliculi.

INTRODUCTION AND MOTIVATION

Despite the fact that bone adaptation is a well-recognized phenomenon in which bones slowly add or lose mass and alter their form in response to alterations in the normal mechanical history, the specific mechanical stimuli that trigger, sustain, and terminate bone adaptation are not presently well characterized or understood. Cyclic loading of bone over and above normal homeostatic stimulus clearly alters the microscale environment in which osteocytes (cells postulated to sense mechanical signals) reside.[6,10] While the macroscopic stress magnitudes and cyclic loading frequencies that produce positive bone adaptation have been identified[32−35] the microscale stimuli to which osteocytes respond are not yet understood.

Over the past decades numerous phenomena associated with load-induced fluid flow and deformation in bone[8] have been postulated as mechano–transduction mechanisms for positive bone adaptation, a good discussion of which is provided by Knothe Tate.[22] Piekarski and Munro[31] and more recently Wang *et al.*,[44] for example, postulated a chemical mechanism based on the notion that load-induced fluid flow in bone enhances the rate of nutrient supply and waste removal to and from osteocytes, thereby providing a more favorable environment for production of additional bone mass. The observation of strong frequency-dependent electric potential gradients in the vicinity of Haversian canals of cortical bone undergoing different types of loading[4,18,39] have added support for flow-related electrical mechanisms due either to fluid flow in the pores of the hydroxyapatite matrix[3,36,37] or flow in the larger canaliculi. Alternatively, it has been proposed that oscillating flow of viscous bone fluids exert stimulatory shear stresses on the osteocytes[19] or their processes.[45] A model for quantifying drag forces and strains in the pericellular matrix of canaliculi due to load-induced fluid flow was developed and exercised by You *et al.*[46] who then postulated "large" strains in the matrix to be another potential mode of osteocyte stimulation. Still further works have been aimed at determining whether or not the fluid pressures in bone during physiological dynamic loadings could possibly serve as the stimulus to which osteocytes respond.[16,47,48] The possibility of bone cells experiencing strain and responding thereto have also been considered, for example by Rubin and Lanyon.[34]

In considering the potential role of load-induced fluid flow in the adaptive response of bone to mechanical stimulus, the length scale of greatest interest is that of the bone cells since that is the level at which mechanical signals

---

are perceived and biological responses initiated. To better understand the range of stimuli experienced by bone cells *in vivo* during mechanical excitation of a whole bone specimen, there is a need for realistic multiscale modeling tools that can take macroscopic whole bone loads (as from walking or running) and determine the nature of stimulus provided to bone cells on the micro and nanoscales. Even under "uniform" stress or strain loading applied to whole bone on the macroscale, the strong heterogeneity in bone morphology leads to corresponding heterogeneity in the resulting stress and strain fields on smaller scales.[27] Computational or analytical micromechanical modeling techniques can take account of specific material heterogeneities to quantify spatially and temporally varying microscale stress and strain fields. A hierarchical modeling of cortical bone's microstructure is undertaken herein, and multiscale modeling techniques are developed and applied to calculate the nature of load-induced fluid flow in the lacunar–canalicular system of bone. The current work is an extension of that by Swan *et al.*[40] in which micromechanically based poroelasticity was used to calculate the nature of fluid flow in the Haversian system of cortical bone prisms subjected to harmonic bending excitations in the range of 10^0–10^6 Hz. Here, a simplified quasi-two-dimensional model is developed and used to facilitate an understanding of the characteristics of load-induced flows in the lacunar–canalicular system.

After the histology of pore systems in cortical bone is briefly reviewed in this article, multiscale analysis methods suitable for cortical bone are introduced, implemented, and then applied. In particular, scale–bridging relations between stresses and strains in the fluid and bone matrix phases on the canalicular length scale and the stresses and strains on the larger lacunar length scale are developed. Beginning on the length scale of individual canaliculi, the strain, stress, and fluid pressure fields that occur under different types of oriented loading of the bone matrix and canaliculi are directly computed using unit cell analysis methods. Appropriate coefficients of a linear, anisotropic poroelasticity model are then chosen to mathematically relate spatially averaged strains, stresses, and fluid pressures in the canalicular system. Moving on to the larger lacunar–canalicular length scale, the load-induced response of an isolated lacuna in a pericanalicular (term storage modulus used here is not to be confused with that in viscoelasticity theory) bone matrix is considered and studied. In this model, pericanalicular bone is modeled with the aforementioned anisotropic poroelasticity model, in which local material directors are aligned with the local direction of canaliculi. After studying the response of an isolated lacuna, the case of a cluster of lacunae scattered about a Haversian canal is then considered and modeled.

MODELING OBJECTIVES

Cortical bone exhibits a rich structural hierarchy.[9,23] Some structural features have been linked to the physical
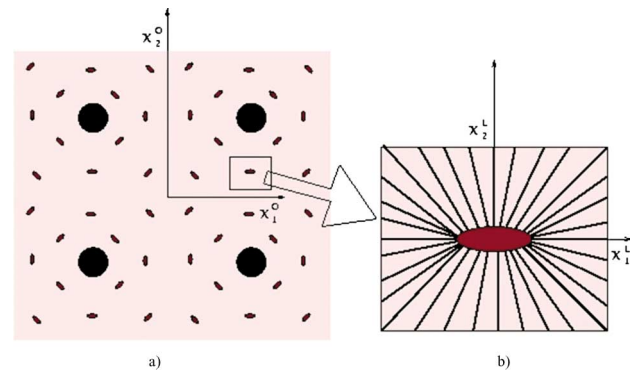

FIGURE 1. (a) Array of Haversian canals with each canal surrounded by a cluster of lacunae; (b) network of canaliculi emanating from a lacuna.

properties of bone. On the largest scale, the tubular shape of long bones is beneficial in attaining the maximum bending and torsion stiffness and strength for a given weight of tissue.[12] On a smaller scale, osteons are cylindrical fibrous structures 200–300 μm in diameter, consisting of concentric lamellae with a Haversian canal at the center.[28] This structure leads to anisotropy of bone.[20] Interfaces between osteons confer a measure of toughness and viscoelasticity to the tissue. Stiffness and strength of bone arises from the composite structure of nanocrystals of calcium phosphate (apatite) mineral and protein (principally collagen) fibers.[21] Structural hierarchy also occurs in the porosity, as follows[7]:

1. Medullary cavities are the grossly cylindrical channels with diameters on the order of up to centimeters that run roughly parallel to the long axis of bones. These cavities are lined with spongy trabecular bone having marrow in the interstices.
2. Haversian canals [Fig. 1(a)] with diameters on the order of 40–100 microns run roughly parallel to the longitudinal axis of bone and roughly down the center of osteons. Analysis of numerous photomicrographs
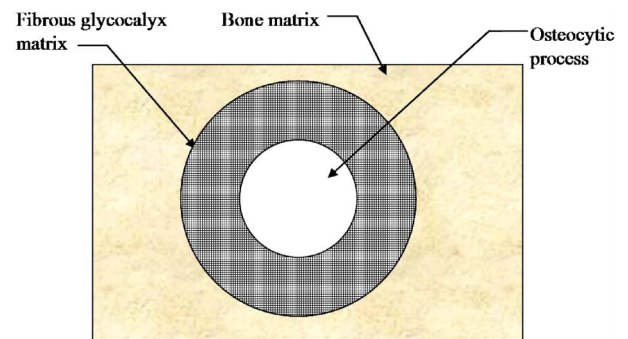

FIGURE 2. An idealized model for the cross section of a canaliculus showing the central region occupied by an osteocytic process and the annular region occupied by fibrous glycocalyx matrix through which fluid flows.

of healthy human cortical bone (e.g., those in Cooper *et al.*[7] Hancox,[17] Martin and Burr,[26] and numerous others) indicates that these channels typically occupy 2–5% of the cortical bone's gross volume; Volkmann canals, similar to Haversian canals except that they run at angles skew to the longitudinal bone axis, are believed to occupy considerably less than 1% of the gross bone volume.

3. Lacunae (Fig. 1) are ellipsoidal cavities in the bone matrix in which osteocytes reside, with major and minor diameters typically of order 30 and 10 microns, respectively, and occupy approximately 2% of the gross cortical bone volume. Micrographs suggest that osteocytes occupy a large fraction ($\geq$50%) of the lacunar volume.[7]

4. Canaliculi (Figs. 1b and 2) are small cylindrical channels with diameters on the order of 0.1 microns that form an anastomosing network connecting individual lacunae and the Haversian/Volksmann vascular canals. Cytoplasmic osteocytic cell processes partially occupy the canaliculi with the remainder occupied by a non-mineralized intralacunar matrix.[28] The canicules (an alternative expression for canaliculi) are estimated by the authors to occupy approximately 1–2% of the cortical bone volume.

5. Pores on the order of 1 nm in size exist in the collagen–hydroxapatite matrix.

In the current modeling effort, the local deformation-induced fluid flow is considered in the neighborhood of a single lacuna. Due to the disparate sizes of lacunae and canaliculi, and due to the large, indefinite number of canaliculi emanating from each lacuna, a homogenization-based modeling approach is taken in which the effective poroelastic properties of the canaliculi and the bone matrix are obtained and then used in modeling deformation-induced flow within the lacunar–canalicular system.

On the length scale of an individual lacuna or even multiple lacunae, the canaliculi form a system of channels with diameters of order $0.1~\mu$m that are here idealized as fanning out radially from each lacuna. Considering a representative section through which one of the canaliculi pass [Figs. 2 and 3(c)], the materials contained in that cross section are the porous collagen–hydroxapatite bone matrix occupying a region denoted Ω_{matrix}, and the contents of the canaliculus occupying the region denoted $\Omega_{\text{canalicus}}$. Although it is accepted that cellular processes from the osteocyte extend into the canaliculi and occupy a significant volume fraction of the canalicular volume,[7,45] the extent to which processes reach into the canicules,[28] the fraction of the canalicular cross section that the processes occupy, and the fiber density in the porous glycocalyx matrix that occupies the annular region between the cell processes and the walls of the canaliculus have been a subject of some uncertainty in bone mechanics. Since resolution of these histological issues is outside the scope of this work, two bounding assumptions regarding the canaliculus contents are invoked

herein and the biomechanical effects associated with each are quantified with the models developed. Specifically, the canaliculi are assumed, on the one hand, to be free of ostoecytic processes and nonmineralized matrix material and fully occupied by a fluid having the same compressibility and viscosity as water. The alternative assumption invoked is that the cell processes extend the full length of the canicules and occupy 50% of the channel cross section. The remaining annular region is assumed occupied by a high-density matrix of actin fibers with water free to seep in the interstices. In model calculations on the lacunar scale, the fluid conductivity characteristics of the canaliculi are varied to accommodate these two disparate possibilities. For simplicity, the micromechanical analysis problem is formulated below on the canalicular length scale with the assumption that the canaliculi are filled with bone fluid. This assumption is subsequently relaxed.

Individual osteocytes occupy an unknown fraction of each lacuna's volume and are believed to attach themselves to the walls of the lacuna through a finite number of nonrigid and changing focal adhesions that are extensions of selected components of the cell's cytoskeleton. The space between an osteocyte and the lacuna wall is believed to be occupied by bone fluids. Key simplifying assumptions invoked here in developing our model of deformation-induced fluid flow in the canalicular–lacunar system are the following:

a) The bone fluid in both the lacuna and the canalicular network has the same physical and rheological properties as water.

b) The osteocyte within the lacuna is not modeled, and accordingly, the lacuna is treated as if it were fully occupied by the bone fluid.

If these assumptions prove overly simplistic, the model can be given more realism in subsequent extensions of this work. However, modeling of an osteocyte would introduce issues (e.g., cell membrane structural properties and permeability, percentage of lacunar occupancy by osteocytes) that we will not address here.

Deformation of a saturated porous material such as bone gives rise to pressure changes and flow of fluid within the communicating pores. As described above, both fluid pressure and flow can have biological consequences. Whether pressure changes or flow predominates will depend on the pore morphology and upon the frequency or time scale at which the deformation is applied.

The classic theory of Biot[1] analyzes the behavior of fluid–solid media in which fluid resides in communicating porosity of a given size. If a load is suddenly applied (as a step function in time) to a slab of such a medium, and the resulting fluid pressure is permitted to dissipate by one-dimensional drainage, the medium will experience a predominantly exponential creep (deformation increases with time t) $\mu = \mu_0 \left(A - B\,\mathrm{e}^{-t/\tau}\right)$ with A and B as constants characteristic of the microstructure of the medium and the
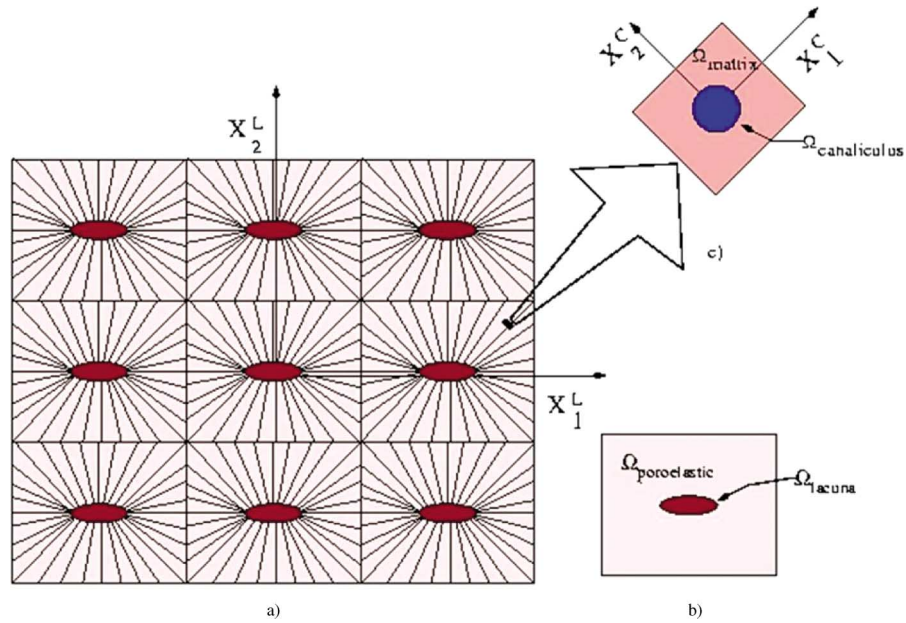
FIGURE 3. (a) Idealized two-dimensional periodic distribution of lacunae; (b) unit cell for lacuna decomposed into poroelastic and lacunar domains; (c) microstructural crosssection of a canaliculus and surrounding collagen–hydroxapatite bone matrix.

relative stiffnesses of the matrix and the pore fluid, and τ as a time constant ($\tau = Ch^2/k$), with k as the permeability, C as another constant and h as the slab thickness (see Ref. 13). A material, which undergoes such exponential creep in the time domain, will under harmonic loading in the frequency domain exhibit a Debye peak in the mechanical damping $\tan \delta$, where δ is the phase angle between stress and strain. This peak in $\tan \delta$ has the following form with $\Delta B/A$ and $B \ll A$, and ω as the angular frequency $\omega = 2\pi f$ in which

f is frequency.[25]

$$\tan \delta = \Delta \frac{\omega \tau}{1 + (\omega \tau)^2}. \tag{1}$$

The meaning of the time constant τ in the context of bone as a biological material is as follows. If physiological deformations are predominantly at time scales longer than τ or at angular frequencies lower than $1/\tau$, then flow predominates and fluid pressure is much lower than the stress in the
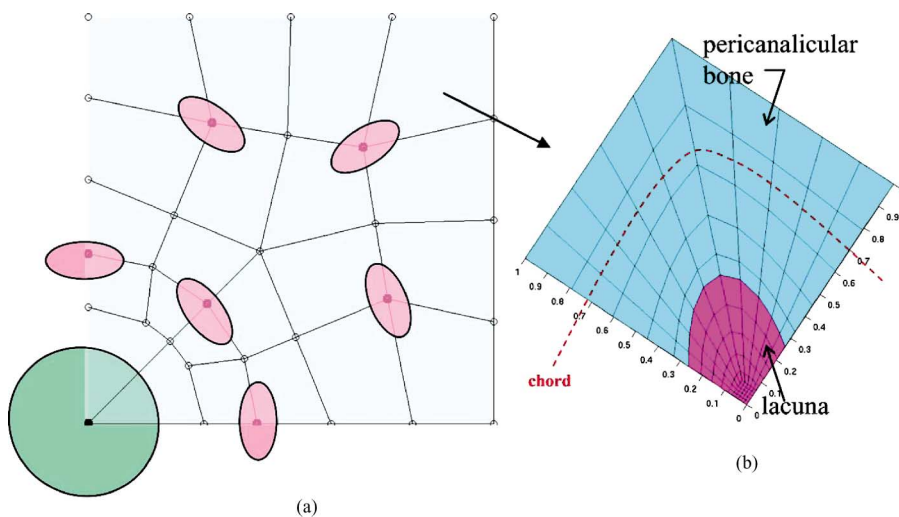

FIGURE 4. (a) Representative background mesh of quadrilaterals for quarter unit-cell model; (b) STC mesh of one of the background quadrilaterals with a segment of an elliptical core.

solid. If physiological deformations are predominantly at time scales shorter than τ or at angular frequencies higher than $1/\tau$, then flow is minimal but fluid pressure is relatively large, though not necessarily as large as the stresses in the bone matrix, since the fluid has insufficient time to be squeezed out. At intermediate time scales or frequencies, the material exhibits a peak in mechanical damping. Anticipating that load-induced fluid flow will occur on multiple length and time scales in bone due to the hierarchy of the pore system, one of the specific aims of this work is to find the range of characteristic relaxation times associated with pore fluid pressure dissipation in bone.

METHODS OF MODELING

Bridging Relations from Canalicular to Lacunar Scale

Modeling is performed on three different length scales herein, and on each different scale, a different set of reference coordinate axes is used. When modeling on the canalicular scale, the reference coordinates of material points are denoted by $\mathbf{X}^{C}$. On the lacunar scale the coordinates are denoted $\mathbf{X}^{L}$ [Fig. 1(b)], and on the osteonal scale by $\mathbf{X}^{O}$ [Fig. 1(a)]. When modeling on the canalicular scale [Fig. 3(c)] the union of the bone matrix and canalicular domains forms what is denoted $\Omega_{\text{pericanalicular}}^{L} = \Omega_{\text{matrix}}^{C} \cup \Omega_{\text{canaliculs}}^{C}$. The bone matrix surrounding each canaliculus is for simplicity modeled as a solid, linearly elastic isotropic material with effective properties consistent with those of a collagen–hydroxapatite composite. While it is in fact realized that the bone matrix is itself a porous, heterogeneous collagen–hydroxapatite composite through which fluids can also flow, the associated material heterogeneity is neglected, for simplicity, when modeling on the canalicular scale, although the hydraulic conductivity through the porous matrix is considered in model computations at the lacunar scale.

When loads are applied to bone, there will exist on the canalicular scale $\ell^{C} \approx O(10^{-1}\mu\text{m})$ spatially varying stress and deformation fields in the vicinity of each canaliculus. Associated with these stress and deformation fields on $\Omega_{\text{pericanalicular}}$, the canalicular-scale displacement field in the solid bone matrix is denoted by $\mathbf{u}^{s}(\mathbf{X}^{C})$, $\forall \mathbf{X}^{C} \in \Omega_{\text{matrix}}^{C}$ and similarly the microscale displacement field in the canalicular fluid by $\mathbf{u}^{f}(\mathbf{X}^{C})$, $\forall \mathbf{X}^{C} \in \Omega_{\text{canaliculus}}^{c}$. The microscale averages of the solid and fluid velocity fields over their respective portions of $\Omega_{\text{pericanalicular}}^{L}$ centered about some point bf $\mathbf{X}^{L}$ on the lacunar scale are computed:

$$\bar{\mathbf{v}}^{s}(\mathbf{X}^{L}) = \frac{\int_{\Omega_{\text{matrix}}^{C}} \mathbf{v}^{s}(\mathbf{X}^{C}, \mathbf{X}^{L}) \, d\Omega}{\int_{\Omega_{\text{matrix}}^{C}} d\Omega};$$

$$\bar{\mathbf{v}}^{f}(\mathbf{X}^{L}) = \frac{\int_{\Omega_{\text{canaliculus}}^{C}} \mathbf{v}^{f}(\mathbf{X}^{C}, \mathbf{X}^{L}) \, d\Omega}{\int_{\Omega_{\text{canaliculus}}^{C}} d\Omega}; \tag{2}$$

The total volume-averaged velocity on the length scale ℓ^{C} provides what is called the *total velocity* of the medium on that scale:

$$\bar{\mathbf{v}}(\mathbf{X}^{L}) = \varphi_{\text{matrix}}^{C} \bar{\mathbf{v}}^{s} + \varphi_{\text{fluid}}^{C} \bar{\mathbf{v}}^{f} \tag{3}$$

In the preceding, $\varphi_{\text{matrix}}^{C}$ and $\varphi_{\text{fluid}}^{C}$ are the respective volume fractions of bone matrix and canalicular fluid volume in the pericanalicular domain $\Omega_{\text{pericanalicular}}^{L}$ on the canalicular scale. Expression (3) above can be rewritten as follows:

$$\bar{\mathbf{v}}(\mathbf{X}^{L}) = \bar{\mathbf{v}}^{s} + \dot{\mathbf{w}} \tag{4}$$

in which

$$\dot{\mathbf{w}}(\mathbf{X}^{L}) = \varphi_{\text{fluid}}^{C}(\bar{\mathbf{v}}^{f} - \bar{\mathbf{v}}^{s}). \tag{5}$$

Written this way, the spatially averaged velocity of the pericanalicular medium about some point $\mathbf{X}^{L}$ has two components: the average velocity of the bone matrix $\bar{\mathbf{v}}^{s}$ and the local *discharge velocity* $\dot{\mathbf{w}}$ which represents the average relative velocity between the canalicular fluid and the bulk medium per unit bulk cross sectional area, and is an indicator of instantaneous fluid flow on the lacunar length scale $\ell^{L} \approx O(10\,\mu\text{m})$. Under "very rapid" loadings applied to pericanalicular bone, there is insufficient time for the fluid in a canaliculus to overcome the viscous and inertial forces that resist flow, thus giving rise to $\dot{\mathbf{w}} \approx \mathbf{0}$. Conversely, under loadings applied relatively slowly or with sufficiently "large duration," there will be ample time for the fluid to overcome viscous and inertial forces that resist flow. However, once excess fluid pressures in a canaliculus have been relieved (i.e., equilibrated) flow ceases once again, returning to the state $\dot{\mathbf{w}} \approx \mathbf{0}$.

The net volumetric rate of fluid flow per gross unit volume into a local region about a point $\mathbf{X}^{L}$ represents a rate of change in volumetric fluid-content. This quantity is denoted by $\dot{\zeta}$ and is available either from canalicular scale inflow rate or lacunar scale divergence of $\dot{\mathbf{w}}$:

$$\dot{\zeta} = \frac{-1}{V} \int_{\Gamma_{f}} \mathbf{n} \cdot \mathbf{v}^{f} \, d\Gamma_{f} \tag{6a}$$

$$= -\nabla_{\mathbf{X}^{L}} \cdot \dot{\mathbf{w}} = -\frac{\partial \dot{\mathbf{w}}_{i}}{\partial X_{i}^{L}} \tag{6b}$$

where, in Eq. (6a), Γ_{f} denotes a bounding surface across which fluid flows; $\mathbf{n}$ represents the outward unit normal vector from the bounding surface; and V denotes a given volume of the pericanalicular bone.

The lacunar-scale strain rate of the poroelastic medium can be related to the canalicular-scale strain rate field and the macroscale velocity field as follows:

$$\dot{\bar{\varepsilon}}(\mathbf{X}^{L}) = \frac{1}{V} \Bigg[\int_{\Omega_{\text{matrix}}} \dot{\varepsilon}^{s}(\mathbf{X}^{C}, \mathbf{X}^{L}), d\Omega_{\text{matrix}}$$

$$+ \int_{\Gamma_{c-m}} \frac{1}{2} [\mathbf{n} \otimes \mathbf{v}^{s} + \mathbf{v}^{s} \otimes \mathbf{n}] \, d\Gamma_{c-m} \Bigg] \tag{7a}$$

$$= \varphi_{\text{matrix}}^{\text{C}} \dot{\bar{\varepsilon}}^{\text{s}} + \varphi_{\text{fluid}}^{\text{C}} \dot{\bar{\varepsilon}}^{\text{canaliculus}} \tag{7b}$$

$$= \frac{1}{2}\left(\nabla_{\mathbf{X}^{\text{L}}} \bar{\mathbf{v}} + \bar{\mathbf{v}} \nabla_{\mathbf{X}^{\text{L}}}\right) \tag{7c}$$

$$= [\dot{\bar{\varepsilon}}_{11}, \dot{\bar{\varepsilon}}_{22}, \dot{\bar{\varepsilon}}_{33}, \dot{\bar{\gamma}}_{23}, \dot{\bar{\gamma}}_{31}, \dot{\bar{\gamma}}_{12}] \tag{7d}$$

In Eq. (7a) $\mathbf{n}$ again represents the unit outward normal vector from the edges of a canaliculus, directed into the bone matrix.

On the canalicular scale ℓ^{C} there exist stress fields in the bone matrix $\boldsymbol{\sigma}^{\text{s}}(\mathbf{X}^{\text{C}}) \forall \mathbf{X}^{\text{C}} \in \Omega_{\text{matrix}}^{\text{C}}$ and stress fields in the canaliculus $\boldsymbol{\sigma}^{\text{f}}(\mathbf{X}^{\text{C}}) \forall \mathbf{X}^{\text{C}} \in \Omega_{\text{canaliculus}}^{\text{C}}$. Lacunar-scale stresses $\bar{\boldsymbol{\sigma}}(\mathbf{X}^{\text{L}})$ in pericanalicular bone are spatial averages of the canalicular-scale solid stresses $\boldsymbol{\sigma}^{\text{s}}(\mathbf{X}^{\text{C}}, \mathbf{X}^{\text{L}})$ and fluid stresses $\boldsymbol{\sigma}^{\text{f}}(\mathbf{X}^{\text{C}}, \mathbf{X}^{\text{L}})$ about a point $\mathbf{X}^{\text{L}}$ on the lacunar scale. When referring to lacunar-scale stresses, there are at least three possibilities for describing their apportionment between the fluid and solid phases: the total average stress in the medium at a point $\mathbf{X}^{\text{L}}$ denoted $\bar{\boldsymbol{\sigma}}(\mathbf{X}^{\text{L}})$; the average stress in the solid bone matrix $\bar{\boldsymbol{\sigma}}^{\text{s}}(\mathbf{X}^{\text{L}})$; and the average stress in the fluid $\bar{\boldsymbol{\sigma}}^{\text{f}}(\mathbf{X}^{\text{L}})$. Mathematically, the average stresses in the matrix and canalicular fluid phases are, respectively:

$$\bar{\boldsymbol{\sigma}}^{\text{s}}(\mathbf{X}^{\text{L}}) = \frac{\int_{\Omega_{\text{matrix}}^{\text{C}}} \boldsymbol{\sigma}^{\text{s}}(\mathbf{X}^{\text{C}}, \mathbf{X}^{\text{L}}) \, d\Omega_{\text{matrix}}^{\text{C}}}{V_{\text{matrix}}};$$

$$\bar{\boldsymbol{\sigma}}^{\text{f}}(\mathbf{X}^{\text{L}}) = \frac{\int_{\Omega_{\text{canaliculus}}^{\text{C}}} \boldsymbol{\sigma}^{\text{f}}(\mathbf{X}^{\text{C}}, \mathbf{X}^{\text{L}}) \, d\Omega_{\text{canaliculus}}^{\text{C}}}{V_{\text{canaliculus}}}; \tag{8}$$

At a point $\mathbf{X}^{\text{L}}$ on the lacunar scale, the average fluid pressure $\bar{\text{p}}^{\text{f}}$ is related to the averaged fluid stress tensor as:

$$\bar{\text{p}}^{\text{f}} = -\frac{1}{3} \text{tr}(\bar{\boldsymbol{\sigma}}^{\text{f}}). \tag{9}$$

The total average stresses at a point $\mathbf{X}^{\text{L}}$ in pericanalicular bone are the volume-weighted sum of the stresses in the fluid and solid phases

$$\bar{\boldsymbol{\sigma}} = \varphi_{\text{solid}}^{\text{C}} \bar{\boldsymbol{\sigma}}^{\text{s}} + \varphi_{\text{fluid}}^{\text{C}} \bar{\boldsymbol{\sigma}}^{\text{f}} \tag{10}$$

which shows that any two of the three average stresses uniquely determine the third.

For pericanalicular bone, the generalized state of deformation at a point $\mathbf{X}^{\text{L}}$ is given by $\bar{\varepsilon}$ and ζ with the corresponding generalized state of stress by $\bar{\boldsymbol{\sigma}}$ and $\bar{\text{p}}^{\text{f}}$. The seven generalized stress variables on the lacunar scale can be related to the seven generalized strain variables on the lacunar scale through the following linear mathematical relationship analogous to those of below[1,2,3]

$$\begin{bmatrix} \bar{\boldsymbol{\sigma}} \\ \bar{\text{p}}^{\text{f}} \end{bmatrix} = \begin{bmatrix} \mathbf{C} & \mathbf{G} \\ \mathbf{G}^{\text{T}} & Z \end{bmatrix} \cdot \begin{bmatrix} \bar{\varepsilon} \\ \zeta \end{bmatrix} \tag{11a}$$

$$\begin{bmatrix} \bar{\varepsilon} \\ \zeta \end{bmatrix} = \begin{bmatrix} \mathbf{S} & \mathbf{B} \\ \mathbf{B}^{\text{T}} & A \end{bmatrix} \cdot \begin{bmatrix} \bar{\boldsymbol{\sigma}} \\ \bar{\text{p}}^{\text{f}} \end{bmatrix} \tag{11b}$$

in which, the terms of $\mathbf{C}$, a symmetric 6×6 matrix, comprise the undrained poroelastic stiffness tensor of pericanalicular bone, and $\mathbf{G}$, a 6×1 matrix, captures the coupling between change in fluid content and change in total stress, and Z, a scalar, is the *storage modulus* (the term storage modulus used here is not to be confused with that in viscoelasticity theory) that denotes the coupling between change in fluid pressure and change in fluid content with strain held fixed. Similarly, the terms of $\mathbf{S}$ represent the fully drained elastic compliance of the bone, while those of $\mathbf{B}$ give the change in fluid content needed to completely relieve fluid pressure under specified applied total stresses. The poroelastic parameter A gives the change in fluid content per unit change in fluid pressure with the total stress $\bar{\boldsymbol{\sigma}}$ held constant. These moduli and compliances are naturally dependent upon the stiffness properties of the bone matrix and those of the bone fluid, their respective microstructural arrangements, and their respective volume fractions.

Quasi-static analysis is performed on the canalicular scale as follows. A unit cell model of the region shown in Fig. 3(c) is developed in which the bone matrix is modeled as isotropic and linearly elastic ($E_{\text{bonematrix}} = 11$ GPa; $\nu_{\text{bonematrix}} = 0.38$). A fluid-filled canaliculus, which occupies 2% of the model volume, contains a Newtonian fluid ($K_{\text{fluid}} = 2.1$ GPa; $\mu_{\text{fluid}} = 10^{-3}$ Pa·s). The remainder of the canalicular scale model is occupied by the bone matrix. The model is subjected to a number of different loading conditions. For example, an average strain $\bar{\varepsilon}_{11}$ is applied to the model, and the resulting equilibrium stress σ, strain ε, and displacement fields in the model are computed. The corresponding averaged stresses, strains, fluid pressure, and change in fluid content are computed in accordance with Eqs. (6–9). This process is then repeated separately for applied averages strains $\dot{\bar{\varepsilon}}_{22}$, $\dot{\bar{\varepsilon}}_{33}$, $\dot{\bar{\gamma}}_{23}$, $\dot{\bar{\gamma}}_{31}$, and $\dot{\bar{\gamma}}_{12}$, Then, the poroelastic moduli of Eq. (11) that relate stress variables ($\bar{\boldsymbol{\sigma}}$, $\bar{\text{p}}^{\text{f}}$) to generalized deformation variables ($\bar{\varepsilon}$, ζ) are computed.

In finding the effective poroelastic properties of the pericanalicular bone, it is worth noting the geometrical similarity between Haversian canals and canaliculi, since both are relatively long (the canals are "long" in that their length to diameter ratios are "large" or $\gg$1.) cylindrical channels embedded in the bone matrix that facilitate transport and fluid flow. Swan *et al.*[42] modeled Haversian bone as a transversely isotropic poroelastic continuum whose effective properties were estimated using the same micromechanical homogenization techniques that are employed here on the canalicular scale to estimate the effective poroelastic moduli of the pericanalicular bone.

Poroelastic Formulation on Lacunar Scale

Considering the bone microstructure in the vicinity of an individual lacuna, the schematics of Figs. 1(b) and 3(a) indicate that a web of canaliculi emanates outward from each lacuna and that this web eventually merges with those for neighboring lacunae. To model and study the load-induced

fluid stresses and flows within the canalicular/lacunar system, an array of lacunae arranged in a regular fashion as shown in Fig. 3(a) will be assumed. For this assumed periodic array of lacunae, the unit cell of the system denoted Ω_s^L is shown in Fig. 3(b) and can be decomposed into the lacuna region Ω_{lacuna}^L and the surrounding poroelastic pericanalicular bone region $\Omega_{\text{poroelatic}}^L$.

Within $\Omega_{\text{poroelastic}}^L$ the pericanalicular bone can be modeled as an anisotropic poroelastic medium. Accordingly, the quasi-static equilibrium of the bulk porous medium (both the bone matrix and canalicular fluid) and that of the fluid relative to the rest of the medium can be expressed when both inertial effects and body forces are negligible, respectively as:

$$\bar{\sigma}_{ij,j} = 0 \qquad (12a)$$

$$-\bar{P}_j^f - R_{ji}\dot{\bar{w}}_i = 0 \qquad (12b)$$

where the range of indices i and j is 1, 2, 3. In Eq. (12), expressions of the form $(*)_{,i}$ are shorthand for $\partial(*)/\partial X_i^L$ and are thus spatial derivatives on the lacunar length scale. Also, in Eq. (12b) the operator denoted R_{ji} is the flow resistivity tensor of the pericanalicular medium that is simply the matrix inverse of the permeability tensor. The constitutive behavior of the poroelastic canalicular medium is described by the mathematical form given in Eq. (11a). When modeled at the lacunar scale ℓ^L the material directors, which describe the orientation of the anisotropic material in the relevant reference frame (i.e., the lacunar scale coordinate system), will vary from point to point in a manner consistent with the local orientation of the canaliculi.

When a macroscopic strain state is imposed on the unit cell Ω_s^L along with periodic boundary conditions, the equilibrium microscale strain field on the domain of Ω_s will be heterogeneous due to the material heterogeneity within the domain of the unit cell. Heterogeneity of the strain field will give rise to gradients of fluid pressure in the canaliculi, and in the lacuna. The nature of the resulting fluid flows that occur between the canalicular and lacunar systems will be modeled and studied.

Since the first objective of the current work is to compute the nature of fluid flow strictly in the neighborhood of a single lacuna, a square periodic array of lacunar unit cells [Fig. 3(a)] is assumed. For the assumed periodic array of lacuna unit cells, analysis can be performed on a single unit-cell model [Figs. 3(b) and 5] if proper periodic boundary conditions are applied. Later in this work, deformation-induced fluid flow amongst multiple lacunae clustered about a Haversian canal is considered.

For the unit cell model of a lacuna and the surrounding poroelastic pericanalicular bone matrix, it is assumed that the heterogeneous stress, strain, and change of fluid-content fields in adjoining unit cells are identical. This implies that each of these fields is periodic and can thus be decomposed

into mean and fluctuating components:

$$\bar{\sigma}(\mathbf{X}^L) = \bar{\bar{\sigma}} + \bar{\sigma}^*(\mathbf{X}^L); \quad \bar{\varepsilon}(\mathbf{X}^L) = \bar{\bar{\varepsilon}} + \bar{\varepsilon}^*(\mathbf{X}^L) \qquad (13)$$

$$\bar{p}^f(\mathbf{X}^L) = \bar{\bar{p}}^f + \bar{p}^{f*}(\mathbf{X}^L); \quad \zeta(\mathbf{X}^L) = \bar{\zeta} + \bar{\zeta}^*(\mathbf{X}^L) \qquad (14)$$

where in the preceding the means are computed by averaging over the lacunar unit cell:

$$\bar{\bar{\sigma}} = \frac{\int_{\Omega_s^L} \bar{\sigma}(\mathbf{X}^L)\, d\Omega_s^L}{\int_{\Omega_s^L} d\Omega_s^L}; \quad \bar{\bar{\varepsilon}} = \frac{\int_{\Omega_s^L} \bar{\varepsilon}(\mathbf{X}^L)\, d\Omega_s^L}{\int_{\Omega_s^L} d\Omega_s^L} \qquad (15)$$

$$\bar{\bar{p}}^f = \frac{\int_{\Omega_s^L} \bar{p}^f(\mathbf{X}^L)\, d\Omega_s^L}{\int_{\Omega_s^L} d\Omega_s^L}; \quad \bar{\zeta} = \frac{\int_{\Omega_s^L} \zeta(\mathbf{X}^L)\, d\Omega_s^L}{\int_{\Omega_s^L} d\Omega_s^L}. \qquad (16)$$

It follows from Eq. (13) that the total displacement field on the lacunar unit cell domain satisfies the following decomposition:

$$\bar{\mathbf{u}}(\mathbf{X}^L, t) = \bar{\bar{\varepsilon}}(t) \cdot \mathbf{X}^L + \bar{\mathbf{u}}^*(\mathbf{X}^L, t). \qquad (17)$$

In strain-controlled unit cell analysis of heterogeneous poroelastic media, a history of macroscopic strain $\bar{\bar{\varepsilon}}(t)$ and average fluid content change $\bar{\zeta}(t)$ are imposed on the unit cell model for $t \in [0, T]$. If one imposes the specific condition that there be no net change in the fluid content of the lacunar unit cell model $[\bar{\zeta}(t) = 0 \,\forall\, t]$ it follows that

$$\int_{\Gamma_s^L} \mathbf{n} \cdot \bar{\mathbf{w}}(\mathbf{X}^L, t)\, d\Gamma_s^L = 0 \qquad (18)$$

a condition that is satisfied if $\bar{\mathbf{w}}(\mathbf{X}^L, t)$ is a spatially periodic function. Spatial periodicity of $\bar{\mathbf{w}}(\mathbf{X}^L, t)$ permits fluid to cross the boundaries of the unit cell model, but permits no net change of fluid content.

In this work, the coupled equations of linear momentum balance for the fluid and solid in the poroelastic domain [Eq. (12)] represent a set of coupled parabolic partial differential equations to be solved for the displacement fields $\bar{\mathbf{u}}(\mathbf{X}^L, t)$ and $\bar{\mathbf{w}}(\mathbf{X}^L, t)$ for $(\mathbf{X}^L, t) \in \Omega_s \otimes [0, T]$. These equations are solved using a poroelastic finite element formulation implemented in the code FENDAC.[40] At a given time $t_n \in [0, T]$ it is assumed that equilibrium fields $\bar{\mathbf{u}}(\mathbf{X}^L, t_n)$, $\bar{\mathbf{w}}(\mathbf{X}^L, t_n)$ that satisfy weak forms of Eqs. (11) and (12) have been obtained. To obtain the solution at time $t_{n+1} = (t_n + \Delta t) \in (0, T)$, the predictor displacement fields on the unit cell model at time t_{n+1} associated with a macroscopic strain condition $\bar{\bar{\varepsilon}}(t_{n+1})$ are as follows:

$$\tilde{\bar{\mathbf{u}}}_{n+1}(\mathbf{X}^L) = \bar{\mathbf{u}}_n(\mathbf{X}^L) + [\bar{\bar{\varepsilon}}(t_{n+1} - \bar{\bar{\varepsilon}}(t_n)] \cdot \mathbf{X}^L \qquad (19a)$$

$$\tilde{\bar{\mathbf{w}}}_{n+1}(\mathbf{X}^L) = \bar{\mathbf{w}}_n(\mathbf{X}^L) + (1 - \alpha)\Delta t_{n+1}\dot{\bar{\mathbf{w}}}_n(\mathbf{X}^L) \qquad (19b)$$

where $\alpha \in (0, 1)$ is a time integration parameter. The strictly periodic corrections to both displacement fields $\bar{\mathbf{u}}^*(\mathbf{X}_L, t_{n+1})$, and $\bar{\mathbf{w}}^*(\mathbf{X}_L, t_{n+1})$ that satisfy the weak form of the field equations at t_{n+1} are then obtained.

Modeling of Fluidic Lacunar Region

While the medium surrounding an individual lacuna can be modeled as poroelastic in keeping with the description above, the fluid in the lacuna is treated as having the constitutive behavior of a viscous Newtonian continuum whose balance of linear momentum in the absence of body forces and inertia forces is governed by

$$\bar{\sigma}^{\text{f}}_{\text{ij},\text{i}} = 0. \tag{20}$$

The local stress in the fluid can be decomposed into a pressure and deviatoric shear stresses as follows:

$$\bar{\sigma}^{\text{f}}_{\text{ij}} = -\bar{p}^{\text{f}}\delta_{\text{ij}} + \bar{\mathbf{s}}^{\text{f}}_{\text{ij}} \tag{21}$$

where the fluid pressure at any point is determined by the compression of the medium and the fluid bulk modulus

$$\bar{p}^{\text{f}} = -K^{\text{f}}\text{tr}(\bar{\varepsilon}^{\text{f}}). \tag{22}$$

The shear stress tensor $\bar{\mathbf{s}}^{\text{f}}$ at any point in the lacuna is determined by the rate of shear deformation tensor $\dot{\bar{\mathbf{e}}}^{\text{f}}$ of the lacunar fluid and the fluid's shear viscosity η^{f}:

$$\bar{\mathbf{s}}^{\text{f}}_{\text{ij}} = \eta^{\text{f}}\dot{\bar{\mathbf{e}}}^{\text{f}}_{\text{ij}}. \tag{23}$$

The volumetric strain $\text{tr}(\bar{\varepsilon}^{\text{f}})$ and the deviatoric strain rate $\dot{\bar{\mathbf{e}}}^{\text{f}}$ in the lacunar fluid are related to the displacement field in the lacuna as follows:

$$\text{tr}(\bar{\varepsilon}^{\text{f}}) = \nabla_{\mathbf{X}^{\text{L}}} \cdot \bar{\mathbf{u}}^{\text{f}} \tag{24a}$$

$$\dot{\bar{\mathbf{e}}}^{\text{f}} = \mathbf{I}_{\text{dev}}\text{:}\left[\frac{1}{2}\left(\nabla_{\mathbf{X}^{\text{L}}}\bar{\mathbf{v}}^{\text{f}} + \bar{\mathbf{v}}^{\text{f}}\nabla_{\mathbf{X}^{\text{L}}}\right)\right] \tag{24b}$$

where $\bar{\mathbf{u}}^{\text{f}}$ and $\bar{\mathbf{v}}^{\text{f}}$ are, respectively, the displacement and velocity fields in the lacunar fluid, and $\mathbf{I}_{\text{dev}}$ is a rank-4 operator that extracts the deviatoric part of a general rank-2 tensor.

Lacuna and Pericanalicular Bone Interface

The lacunar fluid region is modeled as a Newtonian fluid continuum with three displacement components $\bar{u}^{\text{f}}_1, \bar{u}^{\text{f}}_2, \bar{u}^{\text{f}}_3$ for each point $\mathbf{X}^{\text{L}} \in \Omega^{\text{L}}_{\text{lacuna}}$, and the pericanalicular bone region as a poroelastic medium with six displacement components $\bar{u}^{\text{s}}_1, \bar{u}^{\text{s}}_2, \bar{u}^{\text{s}}_3, \bar{w}_1, \bar{w}_2, \bar{w}_3$ for each point $\mathbf{X}^{\text{L}} \in \Omega^{\text{L}}_{\text{poroelastic}}$. It is essential that the proposed model conserve both mass and linear momentum at the moving interface between the lacunar fluid and the poroelastic pericanalicular bone. Conservation of fluid mass can be guaranteed along this interface by satisfaction of the following condition:

$$\int_{\Gamma_{\text{L-p}}} \mathbf{n} \cdot [\rho\dot{\bar{\mathbf{w}}} - \rho(\bar{\mathbf{v}}^{\text{f}} - \bar{\mathbf{v}}^{\text{s}})]\,d\Gamma_{\text{L-p}} = 0 \tag{25}$$

which merely states that the rate of fluid mass flow from the poroelastic canalicular domain toward the moving interface is equal to the fluid mass flow away from the moving interface in the lacunar domain. In Eq. (25), $\mathbf{n}$ denotes the unit normal vector to the lacuna–poroelastic interface pointing into the lacuna, and $\bar{\mathbf{v}}^s$ the velocity of the interface. Since

variations in fluid density across the interface are negligible, Eq. (25) can be satisfied merely by having continuity of the normal fluid velocities relative to the moving interface $\mathbf{n} \cdot \dot{\bar{\mathbf{w}}}$ and $\mathbf{n} \cdot (\bar{\mathbf{v}}^{\text{f}} - \bar{\mathbf{v}}^{\text{s}})$ across the interface.

With conservation of fluid mass satisfied by this equation, a necessary and sufficient condition for conservation of linear momentum across the moving interface is as follows:

$$\int_{\Gamma_{\text{interface}}} \mathbf{n} \cdot [\bar{\boldsymbol{\sigma}}_{\text{pericanalicular}} - \bar{\boldsymbol{\sigma}}_{\text{licunar}}]\,d\Gamma = \mathbf{0} \tag{26}$$

In the preceding expression, $\bar{\sigma}_{\text{pericanalicular}}$ is the total stress on the pericanalicular side of the interface, and $\bar{\sigma}_{\text{lacunar}}$ is the total stress on the lacunar side of the interface.

Hydraulic Conductivity Estimates for Pericanalicular Bone

In poroelastic modeling of pericanalicular bone on the lacunar length scale, it is necessary to estimate effective hydraulic conductivities and resistivities on the lacunar length scale. Since it is difficult to measure such properties through direct experiments, they are generally estimated by modeling fluid flow through the canalicular scale morphology. As noted previously, two sets of morphological assumptions pertaining to the canaliculi are invoked to obtain reasonable bounding estimates of the lacunar scale conductivities of pericanalicular bone. In the first set of assumptions, the canaliculi are modeled as straight circular cylinders fully occupied by a fluid having the viscosity characteristics of bulk water. In the second set of assumptions, the canaliculi are occupied by coaxial osteocytic processes, and a glycocalyx matrix occupies the annular region between the osteocytic process and the wall of the canaliculus. The first assumption leads to an upper-bound estimate of the hydraulic conductivity associated with the pericanalicular bone, whereas the second leads to a lower bound estimate. Later in this work, the permeabilities associated with these two different sets of assumptions are employed in the lacunar scale poroelastic computations.

Fluid-Filled Canaliculi Devoid of Processes and Glycocalyx Matrix

On the lacunar scale, the relation between relative average fluid velocities per gross cross sectional area and average fluid pressure gradients is governed by Darcy's Law:

$$\dot{w}_{\text{i}} = -k_{\text{ij}}(\bar{p}^{\text{f}})_{\text{j}} \tag{27}$$

where k_{ij} denotes the effective permeability tensor of the pericanalicular bone, and $\bar{p}^{\text{f}}$ the averaged fluid pressure as given by Eqs. (8) and (9). In Eq. (27), $(\bar{p}^{\text{f}})_{\text{j}}$ is shorthand for $\partial(\bar{p}^{\text{f}})/\partial X^{\text{L}}_{\text{j}}$ and thus denotes spatial derivatives on the lacunar length scale. The pericanalicular bone permeability can be related to the assumed microstructure of clear, fluid-filled canaliculi by making the assumption of harmonically

oscillating uniaxial fluid flow aligned with the long axis of the canicules as was done by Swan et al.[42] for computing the effective permeability of Haversian bone. Doing so here yields the effective permeability of pericanalicular bone in the direction aligned with the canicules as

$$k_{xx} = \frac{\varphi_{\text{fluid}}^{C}}{\rho^{f}\omega} \left[\frac{2}{\kappa} \frac{I_1(i^{1/2}\kappa)}{I_0(i^{1/2}\kappa)} - i \right] \tag{28}$$

where, I_1 and I_0 are the modified Kelvin functions [2]; $i = (-1)^{1/2}$; ρ^f is the mass density of the canalicular fluid; ω is the frequency at which the flow oscillates; $\kappa = R/\beta = R[\eta^f/(\rho^f\omega)]^{-1/2}$ where R is the cross-sectional radius of the canicules and η^f the shear viscosity of the canalicular fluid. Although the expression of Eq. (28) indicates that the effective permeability under oscillatory flow is generally a complex quantity, for relatively low frequencies with $\kappa \ll 1$, the effective permeability in the canicule direction tends towards a real value $k_{xx} = \phi_{\text{fluid}}^{C} R^2/8\eta^f$ which is the well-known Scheidegger[38] result valid for Poiseuille flow in straight circular canals. For the estimated radius of canaliculi ($R \approx 0.05\ \mu\text{m}$), mass density of water ($\rho_f = 10^3$ kg·m^{-3}) and shear viscosity ($\eta^f = 10^{-3}$ Pa·s), Poiseuille fluid flow in the canaliculi exists and thus the permeability is real so long as the frequency of excitation $\omega \ll 4 \times 10^8$ rad·s^{-1}.

Canaliculi Partially Filled with Processes and Glycocalyx Matrix

A more plausible treatment of the canaliculi by Cowin et al.[11] proposes that the canaliculi are partially occupied by ostoecytic processes, and that the annular region between the processes and the canaliculus wall is occupied by a fibrous glycocalyx matrix through which fluid can seep. Since a lower bound estimate for the pericanalicular permeability is sought here, it is assumed that the glycocalyx matrix has a high density of fibers so that equation of motion governing fluid flow therein is simply Darcy's law (i.e., $\dot{\mathbf{u}} = -\kappa\ \mathbf{grad}\ p_f$) where κ is the effective permeability of the glycocalyx matrix and p_f is the fluid pressure in the matrix. In the model of Tsay and Weinbaum[43] the matrix's permeability is given by the following relation:

$$\kappa = \left[\left(\frac{1}{3}\right) \frac{1}{k_{pl}} + \left(\frac{2}{3}\right) \frac{1}{k_{pz}} \right]^{-1} \tag{29}$$

where:

$$k_{pl} = 0.147\, a_0^2 \left(\frac{\Delta}{a_0}\right)^{2.285} ; \quad k_{pz} = 0.0572\, a_0^2 \left(\frac{\Delta}{a_0}\right)^{2.377} ; \tag{30}$$

Following Cowin et al.[11] it is assumed here that $\Delta \approx$ 7 nm is the characteristic fiber spacing in the glycocalyx matrix in Fig. 2 and $a_0 \approx 0.6$ nm is the fiber radius. These assumptions yield an estimated effective permeability of

the glycocalyx matrix $\kappa \approx 5 \times 10^{-18}$ m^2. Then, assuming that the glycocalyx matrix consumes 75% of the canaliculus cross section, and that the canalicular volume fraction is approximately 0.02, the effective permeability of pericanalicular bone in the direction of canaliculi is estimated at $k_{xx} = 7.5 \times 10^{-20}$ m^2.

The effective permeabilities of pericanalicular bone associated with the two assumptions considered above are provided in Table 2. In essence, the effective permeability based on the assumption of clear fluid-filled canaliculi is ~100 times greater than that associated with a relatively dense glycocalyx matrix.

Energy Considerations. One possible signature of fluid flow in the microstructure of bone under loading is the energy dissipated by the fluid flow. Under steady state harmonic excitation of a bone specimen, the peak elastic strain energy density stored at a given point in the pericanalicular domain is simply the strain energy associated with total stress and strain components that are acting in phase with each other:

$$(U_s)^{\text{canalicular}} = \frac{1}{2}\bar{\sigma}_k \bar{\varepsilon}_k \cos\left(\theta_k^{\bar{\sigma}} - \theta_k^{\bar{\varepsilon}}\right) \tag{31}$$

where $\bar{\sigma}_k$ and $\bar{\varepsilon}_k$ denote, respectively, the absolute values of the kth total stress and strain components at a point $\mathbf{X}^L$ in the poroelastic pericanalicular medium, while $\theta_k^{\bar{\sigma}}$ and $\theta_k^{\bar{\varepsilon}}$ are their respective phase angles between the stress and strain components. Conversely, the total energy dissipated per unit volume at a point in the pericanalicular poroelastic bone model per cycle is E_d and represents the irreversible work done by drag forces in the pericanalicular poroelastic bone matrix against the flowing canalicular fluid. Mathematically the density of energy dissipated per cycle at a point is given as follows:

$$(U_d)^{\text{canalicular}} = (\pi\omega)^2 w_k R_{kj} w_j \tag{32}$$

In the fluidic lacunar region, the peak stored energy density at a point is simply the volumetric strain energy

$$(U_s)^{\text{lacunar}} = \frac{1}{2}K\left(\varepsilon_v^{Lf}\right)^2 \tag{33}$$

while the dissipated energy density per cycle is given by

$$(U_d)^{\text{lacunar}} = \frac{T}{2}\eta\omega^2(\mathbf{e} : \mathbf{e}). \tag{34}$$

In viscoelasticity theory a solid undergoing harmonic loading will have a phase angle δ between stress and strain. The quantity $\tan\delta$ is a useful indicator of the energy dissipated per radian, normalized by the peak energy stored per cycle.[14,25] Using the stored and dissipated energy densities defined above in Eqs. (31–34), $\tan\delta$ is easily computed from its basic definition

$$\tan\delta = \frac{U_d}{2\pi U_s}. \tag{35}$$

where in the preceding expression U_d and U_s are the cumulative dissipated and stored energies in the unit-cell model.

Mesh Generation for Multiple Lacunae Unit Cell Model.
To create a good two-dimensional finite element mesh of a cortical bone specimen containing pericanalicular bone, a Haversian canal, and a cluster of lacunae, the spatial twist continuum (STC) meshing concept of Murdoch *et al.*[29] was employed. Applying the STC methodology to this problem, a coarse background mesh of quadrilaterals was first constructed so that each lacuna was roughly at the center of each. Each of the course quadrilaterals was then subdivided into four using the central coordinate of the lacuna as a vertex for each [Fig. 4(a)]. Chords were then introduced to the mesh as a family of curves that pass consecutively through opposing edges of adjacent quadrilateral elements and such that the existing quadrilaterals were further refined into smaller quadrilaterals [Fig. 4(b)]. The chord arrangements within an STC mesh are shared among neighboring quadrilaterals so that their respective mesh structures will be compatible. Meanwhile, the chords intersecting exterior edges of the quadrant model were flagged to facilitate the one-to-one nodal correspondence of the mesh exteriors. Once the quarter unit cell model was sufficiently well-refined, the remainder of the mesh was created by reflecting the original quadrant about two axes of symmetry.

The anisotropy of the pericanalicular bone surrounding each lacuna is modeled at the individual element level. In each element, the line segment from its centroid to the center of the nearest related lacuna provides the orientation of the canaliculi in that element. In the finite element computations strains are computed within individual elements with respect to the global lacunar scale coordinates [e.g., $\bar{\varepsilon}(\mathbf{X^L})$]. Before the stresses are computed, the strains are rotated into a local coordinate system $\tilde{\mathbf{X}}$ that has the $\tilde{X}_3$ axis is aligned with the canaliculi orientation [e.g., $\tilde{\bar{\varepsilon}} = \mathbf{Q}^T \bar{\varepsilon} \mathbf{Q}$]. In this coordinate system, the constitutive equation Eq. (11) is then applied to calculate the stresses $\tilde{\bar{\sigma}}$ in the local coordinate system. This stress is then transformed back to the global coordinate system as follows: $\bar{\sigma} = \mathbf{Q} \tilde{\bar{\sigma}} \mathbf{Q}^T$.

RESULTS OF COMPUTATIONS PERFORMED

Micromechanical Analysis on Canalicular Scale

A unit cell model of a fluid-filled canaliculus surrounded by isotropic, elastic bone matrix was created. The model was then subjected to a number of strain-controlled loadings under undrained conditions ($\zeta = 0$), and a single fully drained loading ($\bar{p}^f = 0$) and the poroelastic moduli associated with Eq. (11a) were computed. The process followed and results achieved here for pericanalicular bone are completely analogous to those of Swan *et al.*[42] in the context of Haversian bone. The computed poroelastic parameters reported in Table 1 are with respect to a material coordinate system aligned with the canaliculus. When modeling bone at the lacunar scale, the orientation of the canaliculi are position dependent, and accounted for using material directors. The relatively large value of the storage modulus Z here is due to the very small canalicular porosity $\varphi_{canaliculus} = 0.02$ of the medium. To achieve modest changes in bulk fluid content ζ (change in fluid volume per bulk volume of the medium), much larger relative changes in fluid content are required within the individual canaliculi. These larger relative changes of fluid content in the canaliculi in turn create higher canalicular fluid pressures.

TABLE 1. Effective poroelastic moduli and compliances of pericanalicular bone. The X_3 direction is taken as aligned with the canaliculus.

$E_{bonematrix} = 11$ GPa; $\nu_{bonematrix} = 0.38$; $\varphi_{canaliculus} = 0.02$; $D_{canaliculi} = 0.10\ \mu$m

Undrained poroelastic moduli in GPa
All values not reported are zero

$C_{11} = C_{22} = 19.46$;	$C_{12} = C_{21} = 11.85$;	$C_{44} = C_{55} = 3.831$;
$C_{33} = 19.87$;	$C_{23} = C_{32} = 11.93$;	$C_{66} = 3.811$;
	$C_{13} = C_{31} = 11.93$;	

Pore-pressure coupling moduli in GPa
Values not reported are zero

$G_1 = G_2 = -6.515$;	$Z = 68.94$;
$G_3 = -5.280$;	

Fully drained poroelastic compliances in GPa^{-1}
All values not reported are zero

$S_{11} = S_{22} = 9.573 \times 10^{-2}$;	$S_{12} = S_{21} = -3.568 \times 10^{-2}$;	$S_{44} = S_{55} = 2.610 \times 10^{-1}$;
$S_{33} = 9.279 \times 10^{-2}$;	$S_{23} = S_{32} = -3.526 \times 10^{-2}$;	$S_{66} = 2.624 \times 10^{-1}$;
	$S_{13} = S_{31} = -3.526 \times 10^{-2}$;	

Pore-pressure coupling compliances in GPa^{-1}
All values not reported are zero

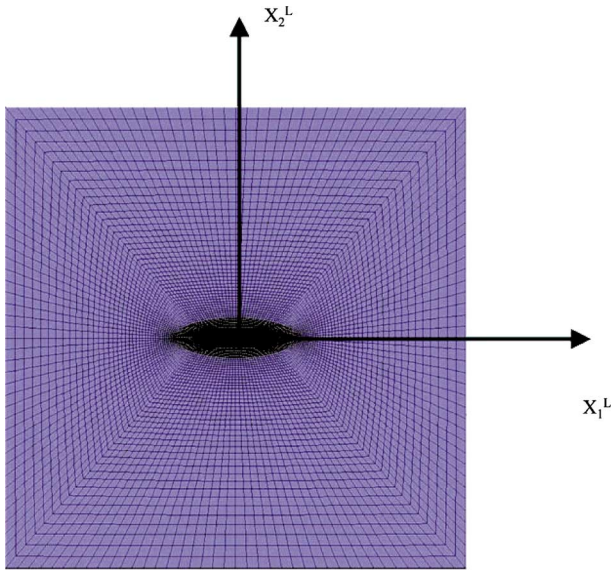|	
$B_1 = B_2 = 2.974 \times 10^{-3}$;	$A = 1.510 \times 10^{-2}$;
$B_3 = 4.416 \times 10^{-4}$	

FIGURE 5. Finely meshed unit cell model containing a single lacuna and the surrounding pericanalicular bone matrix.

These computed effective poroelastic parameters for pericanalicular bone feature stronger anisotropy than may be apparent at first. For example, when a transverse uniaxial strain of $\bar{\varepsilon}_{11}$ is applied under undrained conditions ($\zeta = 0$) the resulting pore fluid pressure is -6.515 GPa $\times \bar{\varepsilon}_{11}$. In contrast, when a uniaxial strain of $\bar{\varepsilon}_{33}$ is applied under undrained conditions, the resulting fluid pressure is -5.280 GPa $\times \bar{\varepsilon}_{33}$. In this sense, when loads are applied in the direction aligned with the long axis of the canaliculi, more moderate fluid pressures are generated. The significance of the anisotropy is even more pronounced when considering the pore pressure compliances in Table 1. Specifically, the coefficients B_1 and B_2 have values of 2.974×10^{-3} GPa^{-1} which means, for example, that if a compressive stress $\bar{\sigma}_{11}$ or $\bar{\sigma}_{22}$ of 1 MPa $= 10^{-3}$ GPa magnitude were applied to the pericanalicular bone, the reduction in fluid content ζ that would be required to relieve the fluid pressure $\bar{p}^{\mathrm{f}}$ would be 2.974×10^{-6}. In contrast, since the coefficient B_3 has a value of 4.416×10^{-4} GPa^{-1}, when a total compressive stress $\bar{\sigma}_{33}$ of the same magnitude is applied to the pericanalicular bone, the required reduction in ζ to completely relieve the fluid pressure $\bar{p}^{\mathrm{f}}$ would be 4.416×10^{-7}. In this way it is apparent that when pericanalicular bone is loaded transversely to the orientation of the canaliculi, larger volumes of fluid flow are generated.

Single Lacuna Unit-Cell Model

"Instantaneous" Undrained Loading Cases

A two-dimensional finite element model (Fig. 5) of the lacunar unit cell corresponding to that in Fig. 1(b) was created. In these computations, the effective poroelastic prop-

erties of the canalicular bone were computed by unit cell analysis and are listed in Table 1 while the lacunar fluid was taken to have the properties of distilled water at 20°C. Using the research finite element code FENDAC[40] homogeneous states of deformation on the osteonal length scale ℓ^{O} were applied to the two-dimensional unit cell model with periodic boundary conditions.[41] Due to the heterogeneity and anisotropy of materials in the lacunar unit cell model, a deformation state homogeneous on ℓ^{O} gives rise to heterogeneous strain, stress, and displacement fields on the lacunar scale ℓ^{L} in order to satisfy balance of linear momentum and mass conservation on this scale. For the poroelastic coefficients of pericanalicular bone (Table 1), and the bounding hydraulic conductivity properties (Table 2), the response of the two-dimensional lacunar unit cell model (Fig. 5) was computed under a number of loading conditions involving separate imposition of quasi-static cyclic strain histories of $\bar{\bar{\varepsilon}}_{11}, \bar{\bar{\varepsilon}}_{22}, \bar{\bar{\gamma}}_{12}$ within the frequency range of 10^0 and 10^6 Hz.

Before considering responses to cyclic loading cases, however, the unit cell model (Fig. 5) was first subjected to a variety of "instantaneous" loading cases to determine the nature of the "undrained" pore pressure fields in the pericanalicular bone and in the lacuna. Accordingly, an instantaneous compressive strain loading of $\bar{\bar{\varepsilon}}_{11} = -1 \times 10^{-5}$ was applied to the model, with all other components vanishing, and the resulting pore pressure field is as shown in Fig. 6(a). Since the applied compressive strain acts parallel to the major axis of the lacuna, a negative fluid pressure develops at the tips of the lacuna ($\bar{p}^{\mathrm{f}} = -.11$ MPa), somewhat larger fluid pressures occur in the pericanalicular bone along the blunt edges of the lacuna ($\bar{p}^{\mathrm{f}} = .17$ MPa), and a modest pressure $\bar{p}^{\mathrm{f}} = .0093$ MPa occurs in the lacuna. In the free-field of the pericanalicular bone, there is modest variation in the fluid pressure field due to the varying orientations of the canaliculi with respect to the direction of loading. Next, an instantaneous compressive strain loading $\bar{\bar{\varepsilon}}_{22} = -1 \times 10^{-5}$ was applied to the model along the minor axis of the lacuna, and the fluid pressure field shown in Fig. 6(b) results. Under this loading, a fluid pressure concentration occurs at the tips of the lacuna ($\bar{p}^{\mathrm{f}} = .29$ MPa) with a large region of negative fluid pressure ($\bar{p}^{\mathrm{f}} = -.075$ MPa) along the blunt edges of the lacuna, and a positive fluid pressure in the lacuna ($\bar{p}^{\mathrm{f}} = .065$ MPa). Last, under an instantaneous shear strain loading $\bar{\bar{\gamma}}_{12} = 2 \times 10^{-5}$ applied to the model, there is no fluid pressure in the lacuna, but large

TABLE 2. Bounding estimates of pericanalicular bone's hydraulic conductivities.

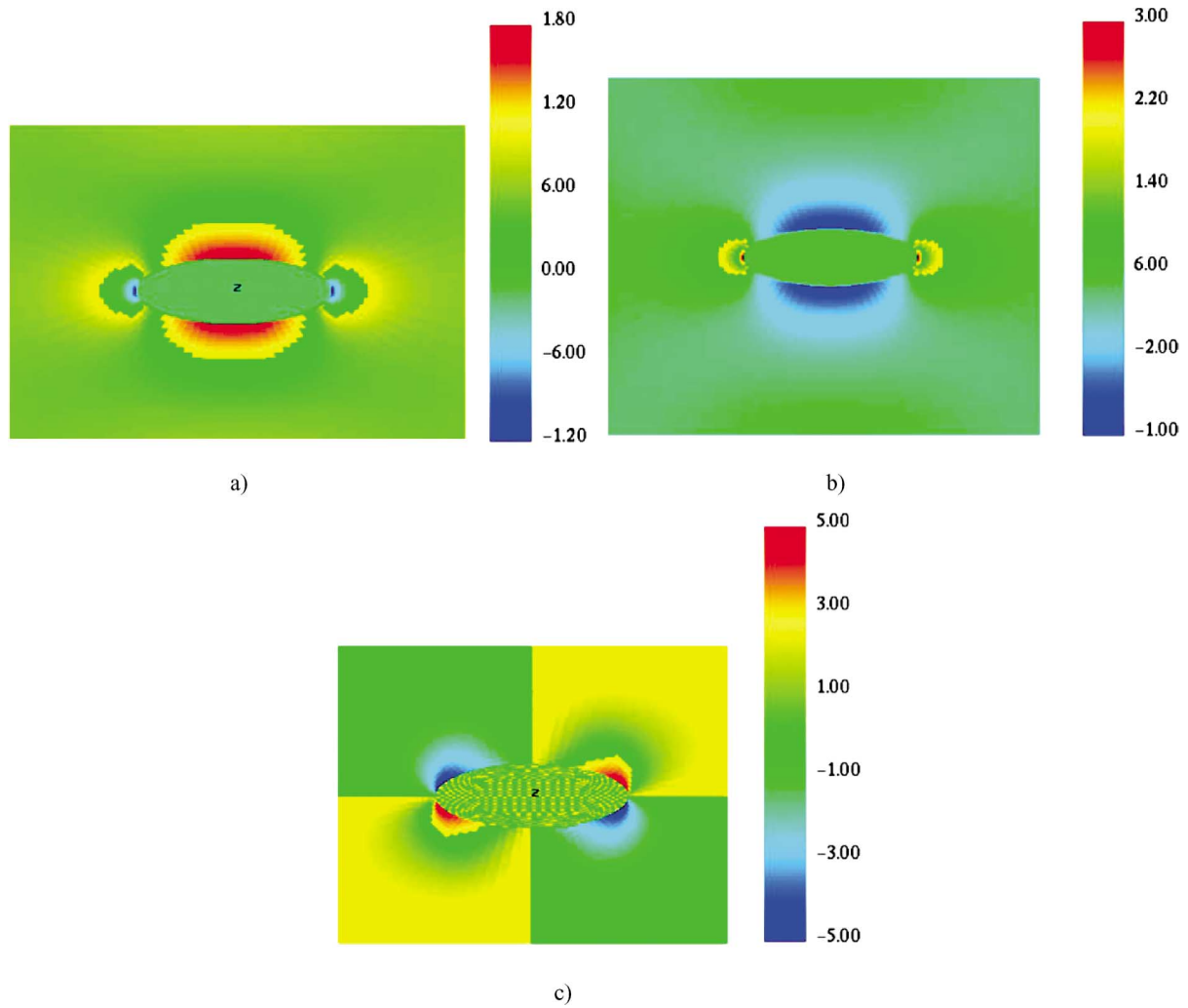|	Axial permeability (m²)	Transverse permeability (m²)
Clear canaliculus assumption	6.7×10^{-18} m²	6.7×10^{-21} m²
Glycocalyx matrix assumption	7.5×10^{-20} m²	6.7×10^{-21} m²

FIGURE 6. Computed fluid pressure distributions in units of dynes $\times$ cm^{-2} $\times$ 10^6 in the vicinity of the fluid-filled lacuna under different types of strain-controlled undrained ($w = 0$) loading conditions. (a) applied loading of $\bar{\bar{\varepsilon}}_{11} = -1 \times 10^{-5}$; (b) applied loading of $\bar{\bar{\varepsilon}}_{22} = -1 \times 10^{-5}$; (c) applied loading of $\bar{\bar{\gamma}}_{12} = 2 \times 10^{-5}$.

positive and negative fluid pressure concentrations of magnitude .48 MPa develop just above and below the tips of the lacuna.

Harmonic Loading Cases

Two series of computed spatial pore fluid pressure distributions in the unit cell model under applied harmonic loadings of $\bar{\bar{\varepsilon}}_{11} = 1 \times 10^{-5}$ at frequencies of 10^0 and 10^2 Hz are shown in Fig. 7. The results shown were generated with lower bound permeability estimates for pericanalicular bone. The spatial distributions of fluid pressure shown are taken at normalized time increments of $(t/T = 0.1)$ where T is the relevant period of loading. When the loading frequency is 10^0 Hz, the computed pore fluid pressures throughout the unit cell are spatially uniform [Fig. 7(a)], whereas at a loading frequency of 10^2 Hz, there are discernible gradients in pore fluid pressure [Fig. 7(b)].

Alternatively, when the same model is subjected to harmonic strain loading of $\bar{\bar{\gamma}}_{12} = 2 \times 10^{-5}$ at frequencies of 10^2 and 10^4 Hz., the resulting computed spatial pore fluid pressure distributions are as shown in Fig. 8. The lower bound permeability estimates for the pericanalicular bone were again used in these computations. At 10^2 Hz, the computed pore fluid pressures throughout the unit cell [Fig. 8(a)] are essentially spatially uniform with the exception of strong pressure concentrations around the sharp curvature regions of the lacuna. At 10^4 Hz, there are very strong transient gradients in pore fluid pressure throughout the unit cell.

Since it is somewhat difficult to gauge the strength of load-induced fluid flows simply by looking at pore fluid pressure distributions, computed tan δ vs. frequency for all three types of harmonic strain-controlled loading cases are presented in Fig. 9 for both upper and lower bound pericanalicular bone permeabilities. For strain-controlled
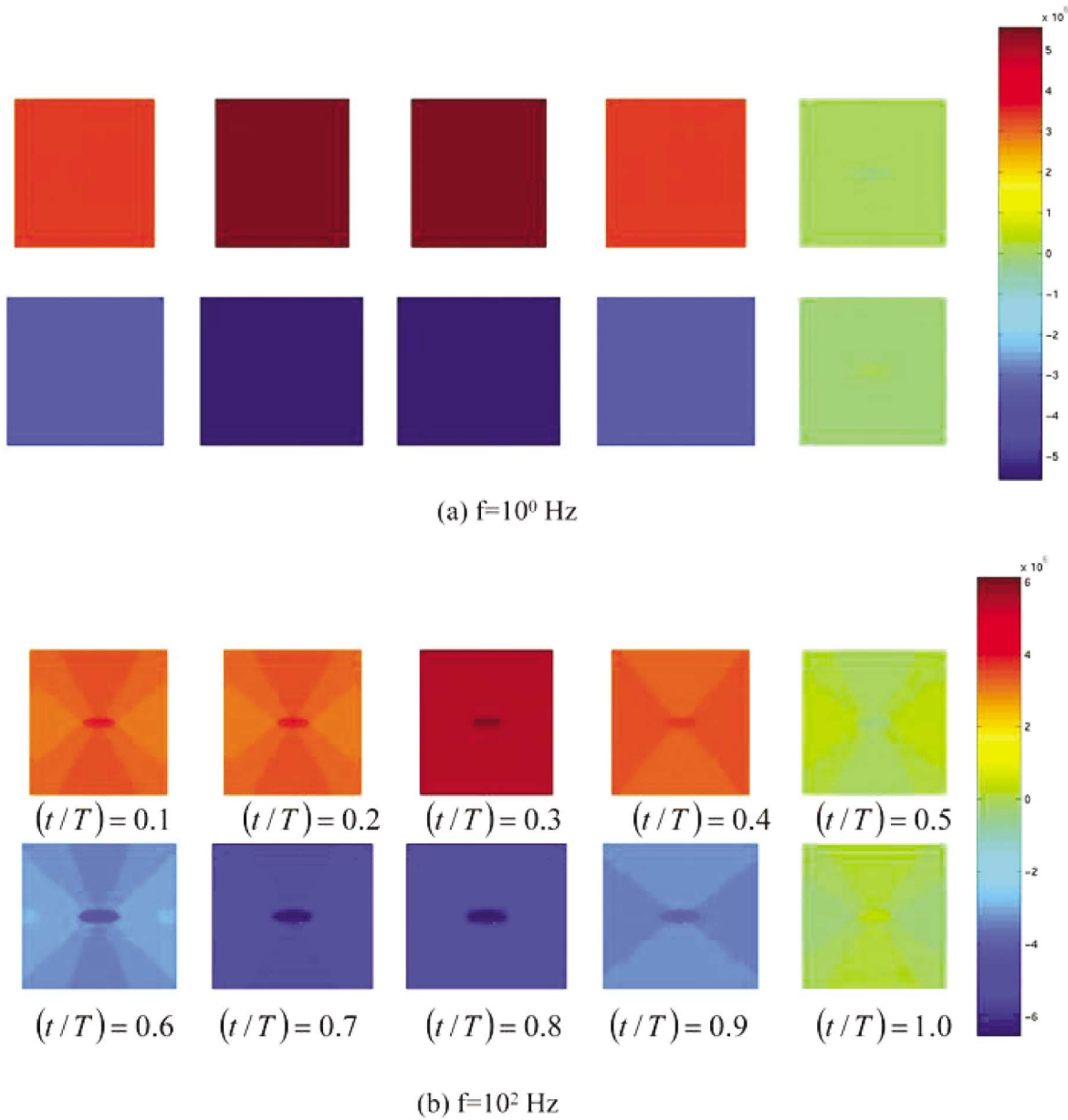
FIGURE 7. Temporal and spatial distributions of computed pore fluid pressure in dynes/cm^2 within a lacunar unit cell model. The lower permeability estimate of the pericanicular system was employed. Loading of the model was by application of a sinusoidal strain $\bar{\bar{\varepsilon}}_{11} = -1 \times 10^{-5}$ at a frequency of (a) 10^0 Hz and (b) 10^2 Hz. Lacunar volume fraction in model shown is 2%. Peak compression of the model occurs at $(t/T) = 0.25$ while peak extension occurs at $(t/T) = 0.75$.

$\bar{\bar{\varepsilon}}_{11}$ loading, the peak tan δ values computed for the model are approximately 6×10^{-3} and occur at frequencies lying between 10^3 and 10^5 Hz, with the lower frequency corresponding to the partially-filled canaliculi assumption. For analogous strain-controlled loading $\bar{\bar{\varepsilon}}_{22}$, the frequencies at which the peaks in tan δ occur are similar, although the magnitudes of the peak values are smaller by roughly an order of magnitude. When strain-controlled harmonic shear loading is applied to the model, the computed peak value of tan δ is approximately 1.2×10^{-3}

but surprisingly, it occurs at significantly higher frequencies than it does for the two extensional loading cases (Fig. 9).

Multiple Lacunae Unit-Cell Model

A more realistic unit cell arrangement of twenty lacunae scattered around a single Haversian canal within an osteon is captured in the second model (Fig. 10). Both the finite element meshing of the lacunae and the surrounding
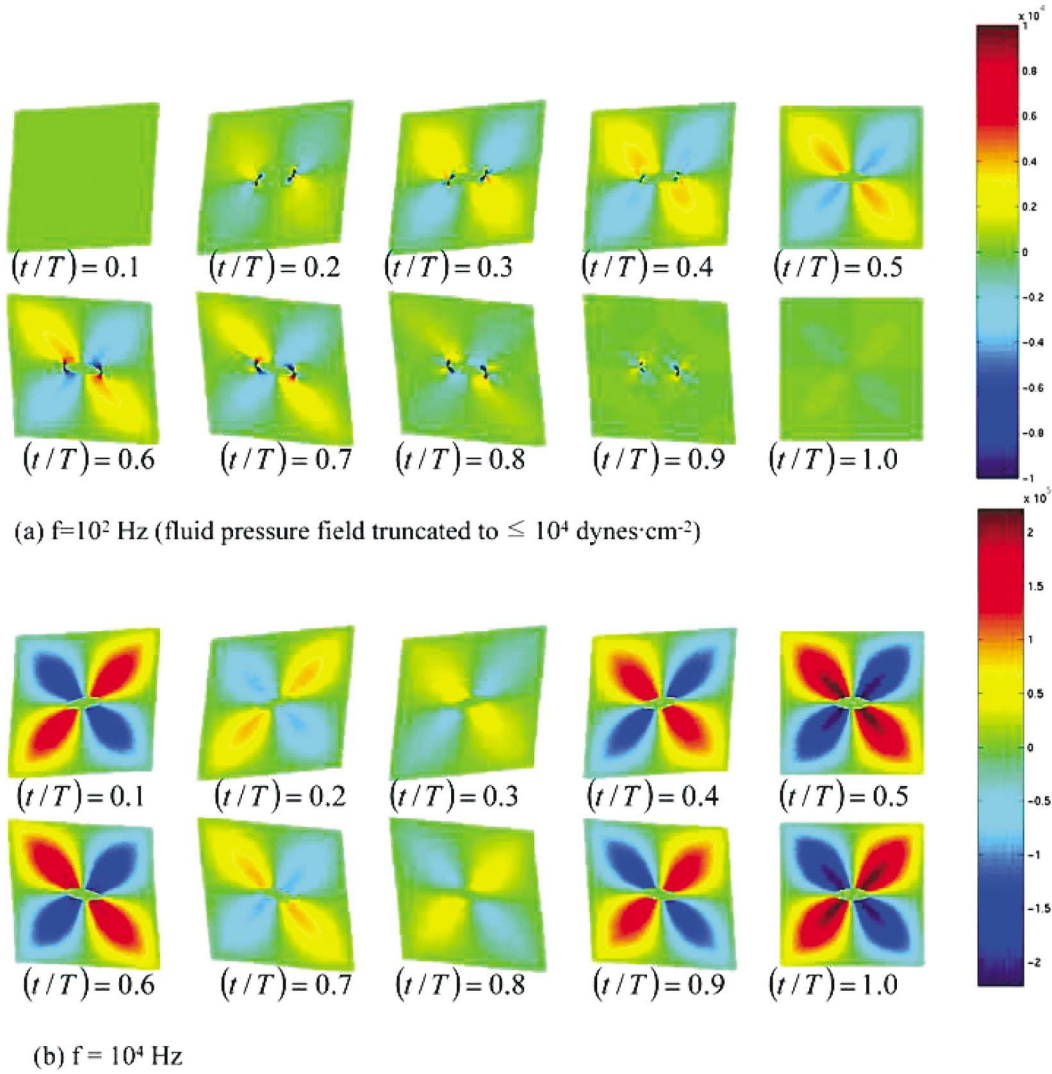
(a) f=10^2 Hz (fluid pressure field truncated to $\leq 10^4$ dynes·cm^{-2})

(b) f = 10^4 Hz

FIGURE 8. Computed spatial and temporal fluid pressure distributions in dynes/cm^2 throughout the lacunar–canalicular unit cell under harmonic shear loadings of magnitude $\bar{\bar{\gamma}}_{12} = 2 \times 10^{-5}$ at (a) $f = 10^2$ Hz; and (b) $f = 10^4$ Hz. The lower estimate of pericanicular permeability was used to obtain the results shown.

bone matrix are shown (left) as well as the local orientation vectors of the canaliculi in the model (right). This model was treated as a unit cell that repeats itself spatially on the osteonal scale. It was subjected to a number of harmonic shear strain-controlled loadings ($\bar{\gamma}_{12} = 2 \times 10^{-5}$) at varying frequencies with periodic boundary conditions applied to the unit cell. In each computation, fluid pressures and the energy dissipated per cycle of loading were quantified.

A sample of the results obtained with this model shows (Fig. 11) the computed fluid pressure distributions in the multilacunae unit cell model during steady state harmonic ($f = 10$ Hz) shear strain loading. The pore pressure distributions feature transient gradients on two length scales: (1) in the bone matrix immediately surrounding individual lacunae [Fig. 11(a)], somewhat analogous to those in

Fig. 8(a), occurring on very short length scales (immediate neighborhoods of the lacunae), with relatively short associated relaxation times; (2) in the regions between lacunae [Fig. 11(b)], and thus featuring more moderate pressure gradients and larger pressure relaxation times. At a loading frequency of 10 Hz and $\bar{\gamma}_{12} = 2 \times 10^{-5}$, peak fluid pressures as large as 10^5 dynes/cm^2 are computed in the pericanicular bone just outside of the lacunae. The computed energy dissipation characteristics associated with this multilacunae unit cell model under shear loading0 (Fig. 12) indicate a very broad tan δ curve with a peak value of 0.004 occuring at $f \approx 7$ KHz when a lower estimate of the pericanicular bone's permeability is employed. Naturally, the frequency at which this peak occurs is much higher for the higher estimate of pericanicular permeability.
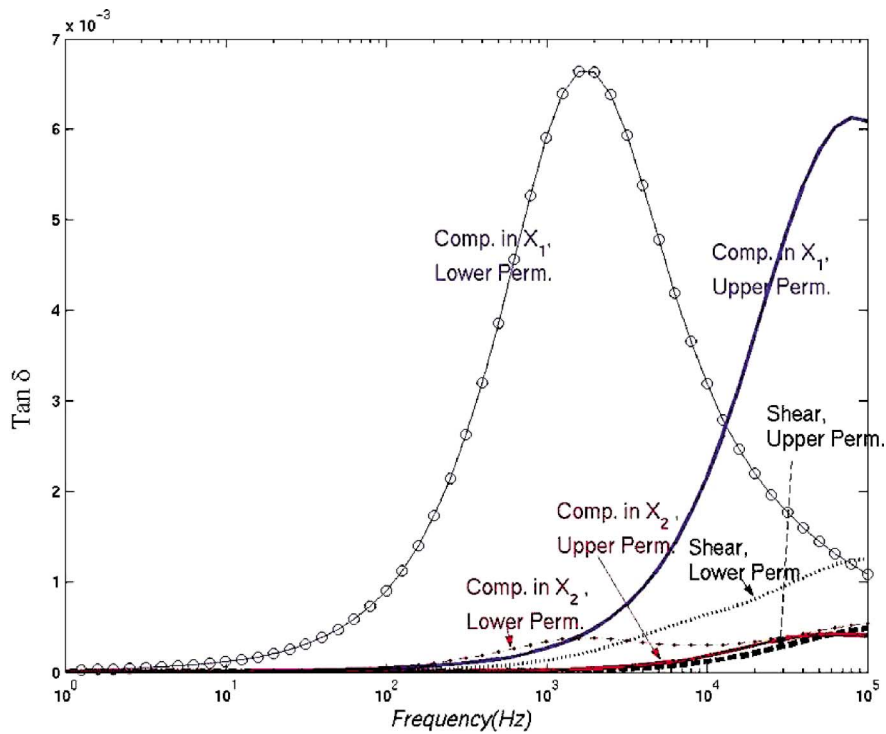
FIGURE 9. Computed tan δ vs. frequency for varying modalities of strain-controlled loading on the single-lacuna unit cell model and for upper- and lower-bounding values of the pericanalicular permeability.

DISCUSSION

The results of the single lacuna unit cell model computations indicate (Fig. 8) that compression and extension of the lacuna along its major axis gives rise to stronger fluid flow and mechanical damping than similar extensional loading along the minor axis or shearing of the lacuna. Indeed, the computed peak mechanical damping due to loading along the major axis of the lacuna is an order of magnitude greater than that associated with loading along the minor axis. The peak damping due to shearing of the lacunar unit cell model is intermediate to that of the preceding cases, but occurs at
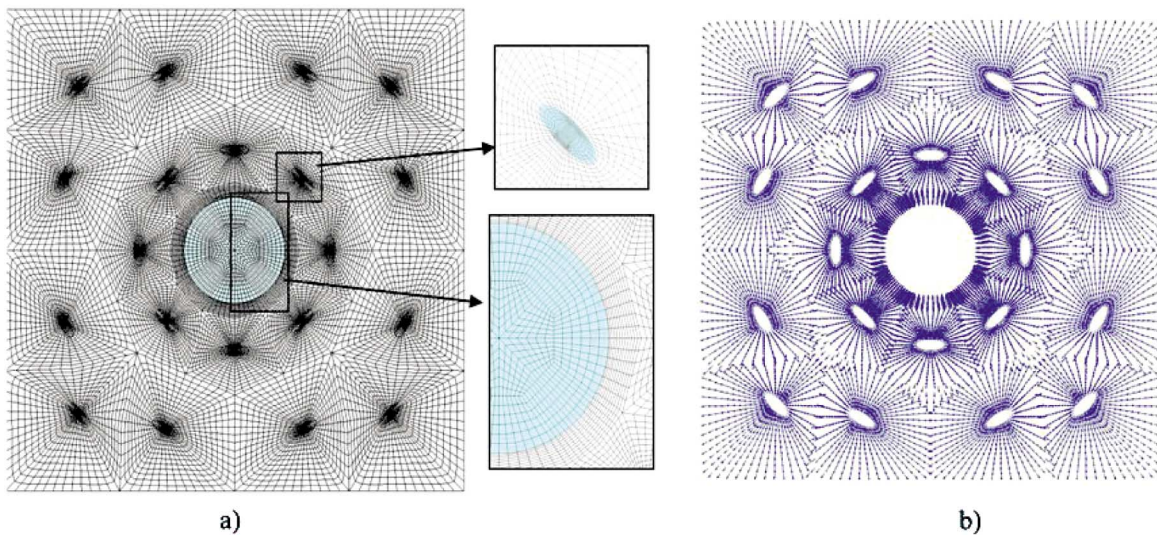

FIGURE 10. (a) Unit cell model containing many lacunae scattered about a Haversian canal; and (b) arrows in each element show local orientations of canaliculi in the model.
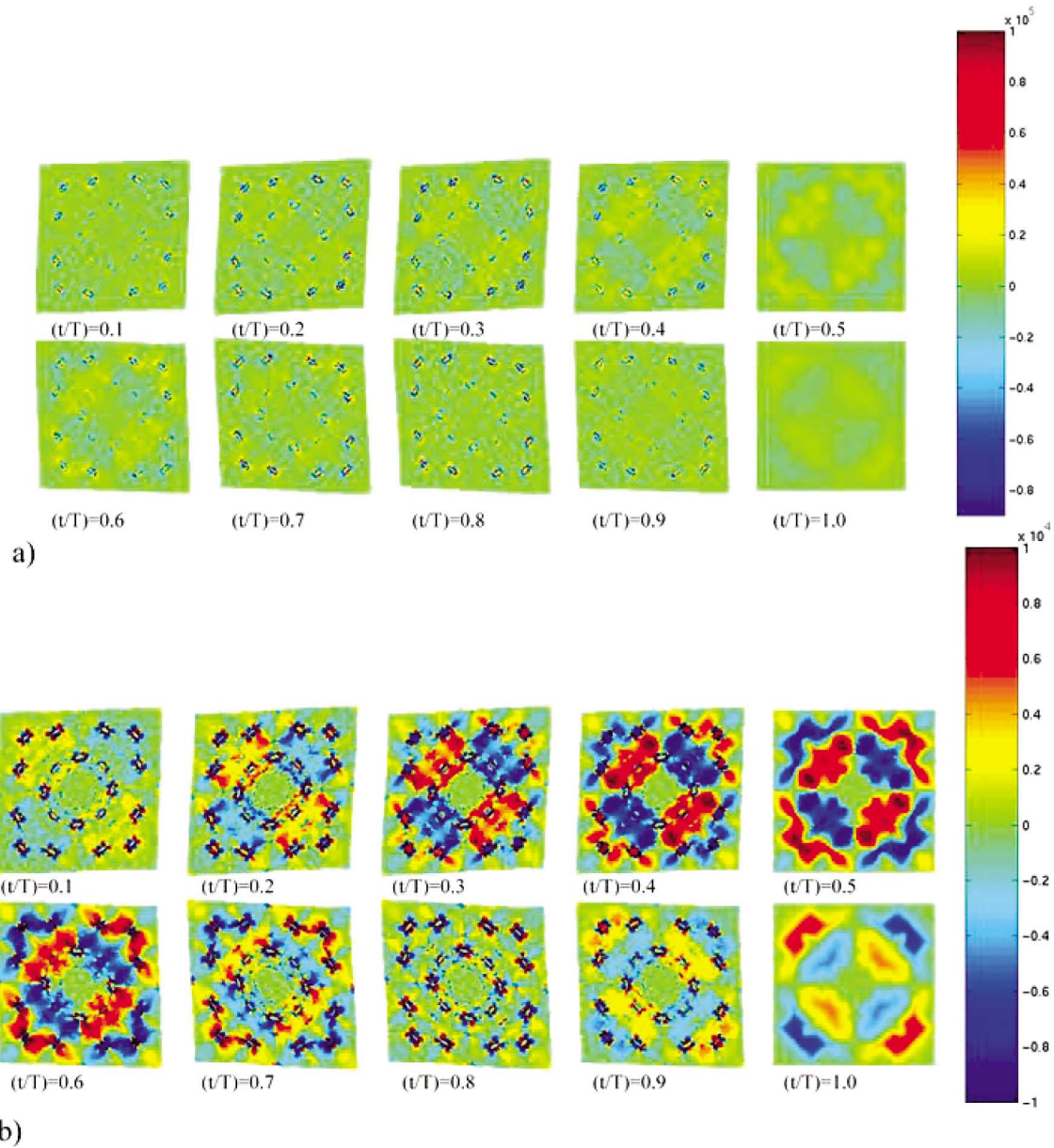
FIGURE 11. (a) Computed spatial fluid pressure distributions in the multilacunar unit cell model under a cyclic shear strain loading of $\bar{\bar{\gamma}}_{12} = 2 \times 10^{-5}$ at $f = 10$ Hz. The pressure distributions are shown at $(t/T) = 0.1, 0.2, 0.3, 0.4, 0.5, 0.6, 0.7, 0.8, 0.9,$ and 1.0. The lower bound peri-canicular permeability was used and the peak fluid pressure is approximately 10^5 dynes cm^{-2}; (b) Same results, but shown with a pressure cutoff of $\pm 10^4$ dynes cm^{-2}.

frequencies nearly two orders of magnitude larger. From these results, it appears that extensional loading of lacunae along their major axes gives rise to a mode of flow that is dominant.

The reason that fluid flow is strongest when the lacunar unit cell model is loaded along the major axis of the lacuna is shown in Fig. 6(b). In this mode of harmonic loading the absolute value of fluid pressure in the lacuna at any given time instant typically exceeds that existing in the surrounding pericanalicular bone at the same time. Furthermore, the

fluid pressure in the lacuna occurs at a slight phase angle that leads the compressive straining of the model. It is also worth noting that as the model is first compressed [$t \in (0.25T)$] during a sinusoidal loading cycle, the canaliculi oriented transverse to the direction of primary compression along the X_1 axis experience larger fluid pressures than those aligned with the X_1 axis. It is easier to see this when the model is loaded at higher frequencies [i.e., at 100 Hz in Fig. 8(b)] than at lower frequencies [i.e., 1 Hz in Fig. 8(a)]. At low frequencies, there is ample time for fluid to flow throughout
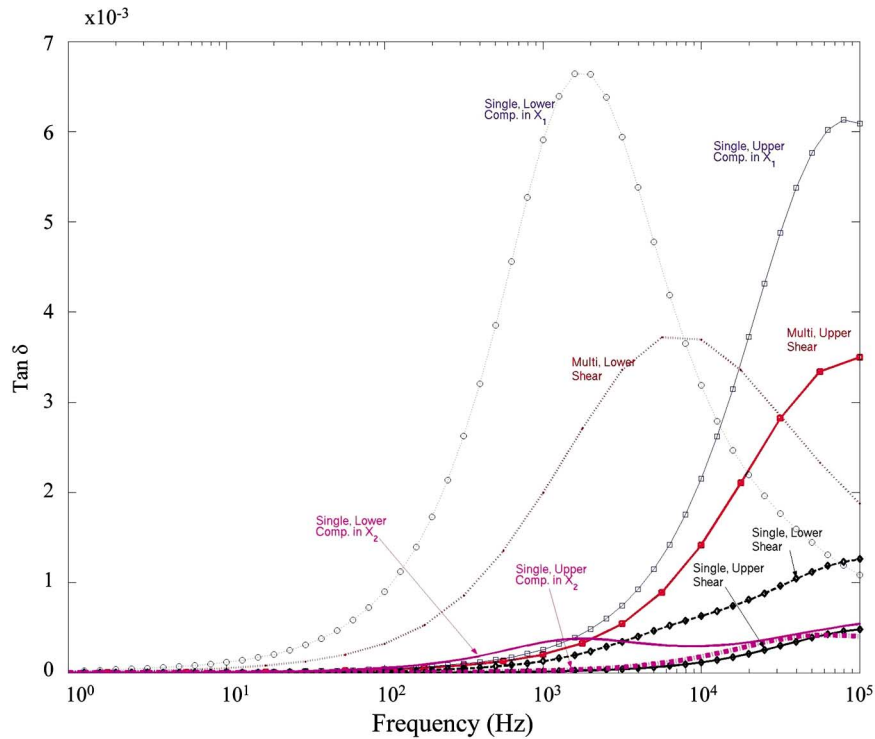
FIGURE 12. Computed tan δ vs. frequency for both single and multilacunae models. In curve identifiers, "single" refers to the single-lacuna unit cell model and "multi" refers to the multilacunae model. The terms "lower" and "upper" refer to upper and lower bounds on the pericanalicular permeability. The last term for each identifier denotes the mode of strain-controlled loading the model was subjected to.

the model and dissipate any pressure gradients, hence the lack of apparent fluid pressure gradients in Fig. 8(a).

The micrographic study of Cooper *et al.*[7] and many contemporary photo-micrographs indicate that in transverse cross sections of cortical bone, lacunae tend to cluster around Haversian canals with their long axes oriented parallel to the lamellae of the osteons in which they are embedded. Accordingly, within a transverse cross section of long bone, one would expect to find lacunae of many orientations as is suggested by the schematics of Figs. 1(a) and 10. Due to the many orientations of lacunae within transverse sections of long bone, virtually any type of loading in the transverse plane will create a situation in which some of the lacunae are sheared, some are stretched/compressed along their minor axes, and others are stretched/compressed along their major axes. With all three types of lacunar-scale loadings occurring simultaneously under virtually any type of mechanical loading applied to cortical bone, it is expected that those lacunae having their major axes aligned with the major axes of loading give rise to the predominant modes of microscale fluid flows and energy dissipation. For a given pericanalicular permeability, the computed curve of tan δ vs. frequency (Fig. 12) for the multilacunae model (Fig. 10) resembles in some sense an averaging of the computed curves for the single-lacuna model under all three modalities of loading

$(\bar{\bar{\varepsilon}}_{11}, \bar{\bar{\varepsilon}}_{22}, \bar{\bar{\gamma}}_{12})$. As a result of this "averaging" the magnitude of the peak tan δ for the multilacunae model under shear loading is only about half that associated with the dominant $\bar{\bar{\varepsilon}}_{11}$ mode of loading, and the peak frequency is intermediate to the peaks associated with extensional and shear loading in the single-lacuna model. These observations are consistent with the fact that only some of the lacunae in the multilacunae model are aligned with the major axes of loading.

For realistic volume fractions of canaliculi and the lower permeability estimates of pericanalicular bone, the models developed and applied here indicate that deformation-induced fluid flow in the pericanalicular system have much larger characteristic time constants ($\tau \approx 10^{-3}$ sec) than fluid flow in the Haversian porosity[42] for which ($\tau \approx 10^{-5}$ sec). The peak mechanical damping predicted here due to flow in the lacunar–canalicular system (0.005) is rather small in comparison with the overall damping measured in bone (a tan δ of 0.02–0.03 near 1 kHz[5,15]). If the peak in damping computed here due to deformation-induced lacunar–canalicular flow is realistic, it would be somewhat difficult to resolve in the experimental results due to the presence of other more dominant damping mechanisms. Nevertheless, with lower bound pericanalicular permeability values employed, the current model results indicate

a definite existence of pressure driven fluid flow in the lacunar–canalicular system under virtually any modality of mechanical excitation above 100 Hz. While fluid flow also occurs under loadings in the more physiological range of 1–100 Hz, the current model predicts that the associated fluid pressures are much smaller.

It is worth noting that the computed fluid pressure relaxation times ($\tau \approx 10^{-3}$ sec) in the lacunar canalicular porosity are quite sensitive to the assumption of fiber spacing in the glycocalyx matrix. While a proteoglycan fiber spacing of 7 nm was assumed herein,[45] alternative spacings of 3 and 18 nm were considered by Wang *et al.*[44] with the smaller spacing resulting in a 10-fold increase of relaxation times, and the larger spacing resulting in a 10-fold reduction. Hence there remains a very considerable degree of uncertainty in pressure relaxation times within the lacunar–canalicular system.

Even for assumed fiber spacing in the glycocalyx matrix of 7 nm, the computed fluid pressure relaxation times in the lacunar–canalicular system from this work are considerably smaller than those computed by others.[44,47,48] This would appear to be due to an assumption of one-dimensional radial fluid flow in the other efforts, where the characteristic drainage distance h is the difference between the radius of an osteon and that of a Haversian canal. As noted above under the assumption of one-dimensional drainage, the relaxation time is given by a relation $\tau = Ch^3/k$. In the current work, the drainage has been multidimensional as opposed to one-dimensional, and this tends to reduce relaxation times considerably. In the current modeling effort the effective drainage distances have also been considerably shorter than those assumed by Wang *et al.*[44] and Zhang *et al.*[47,48] In particular when considering deformation-induced fluid flow in the neighborhood of a single lacuna, the drainage distances are typically only a few tens of microns, since flow is caused primarily by local gradients in pore pressure created by the lacuna. Even when considering deformation induced fluid flow on the osteonal scale (Figs. 10 and 11), the largest fluid pressures tend to occur around the edges of the lacunae, and these appear to be relieved fairly quickly due to the short drainage distances.

The models developed and exercised here have been strictly mechanical in nature, and have not attempted to address potential mechano–electrical effects arising from transport of dissolved ions during deformation-induced interlacunar flow of bone fluids. These effects will need to be addressed in subsequent extensions of this work that must also begin to address the challenge of incorporating mathematical cell models into the framework.

Finally, while microscale models of the type presented here can clearly be developed and exercised, they require microscale anatomical information. When this information is not readily available, assumptions must be invoked, and the validity of these assumptions can be studied indirectly by examining the consistency between model results and macroscopic experimental observations. In this work it has been assumed, for example, that canaliculi from neighboring lacunae communicate with each other, and that fluid can flow among lacunae through this system. It has also been assumed that canaliculi are partially occupied by osteocytic processes with the remainder occupied by a glycocalyx matrix through which bone fluids and flow. Together these assumptions give rise to computed pressure relaxation times ($\tau \approx 10^{-3}$ sec) associated with fluid flow in the lacunar–canalicular system. While not definitive in confirming the anatomical modeling assumptions invoked, the associated pressure relaxation times computed are at least consistent with those measured experimentally by Garner *et al.*[15] and Buechner *et al.*[5] in dynamic excitation of wet bone specimens.

REFERENCES

[1] Biot, M. A. General theory of three-dimensional consolidation. *J. Appl. Phys.* 12:155–164, 1941.
[2] Biot, M. A. Theory of propagation of elastic waves in a fluid-saturated porous solid. II. Higher frequency range. *J. Acoust. Soc. Amer.* 28(2):179–191, 1956.
[3] Biot, M. A., and D. G. Willis. The elastic coefficients of the theory of consolidation. *J. Appl. Mech.* 24:594–601, 1957.
[4] Brankov, G., and R. Blagoeva. An anatomical model for streaming potentials in osteons. *J. Biomech.* 17(8):627–636, 1984.
[5] Buechner, P. M., R. S. Lakes, C. Swan, and R. A. Brand. A broadband viscoelastic spectroscopic study of bovine bone: Implications for fluid flow. *Ann. Biomed. Eng.* 29:719–728, 2001.
[6] Burger, E. H., J. Klein-Nulend, A. van der Plas, and P. J. Nijweide. Function of osteocytes in bone—their role in mechanotransduction. *J. Nutr.* 125:2020S–2023S, 1995.
[7] Cooper, R. R., J. W. Milgram, and R. A. Robinson. Morphology of the osteons. An electron microscopic study. *J. Bone Jt. Surg. Am.* 48:1239–1271, 1966.
[8] Cowin, S. C. Bone stress adaptation models. *J. Biomech. Eng.* 115:528–533, 1993.
[9] Cowin, S. C. Survey article: Bone poroelasticity. *J. Biomech.* 32:217–238, 1999.
[10] Cowin, S. C., L. Moss-Salentijn, and M. L. Moss. Candidates for the mechanosensory system in bone. *J. Biomech. Eng.* 113:191–197, 1991.
[11] Cowin, S. C., S. Weinbaum, and Y. Zeng. A case for bone canaliculi as the anatomical site of strain generated potentials. *J. Biomech.* 28:1281–1297, 1995.
[12] Currey, J. The Mechanical Adaptations of Bones. Princeton: Princeton University Press, 1984.
[13] Djerad, S. E., F. du Burck, S. Naili, and C. Oddou. Analyse du comportement rhéologique instationnaire d'un échantillon de muscle cardiaque. *C. R. Acad. Sci. Paris, série II* 315:1615–1621, 1992.
[14] Ferry, J. D. Viscoelastic Properties of Polymers. New York: Wiley, 1980.
[15] Garner, E., R. Lakes, T. Lee, C. Swan, and R. Brand. Viscoelastic dissipation in compact bone: Implications for stress-induced fluid flow in bone. *J Biomech. Eng.* 122:166–172, 2000.
[16] Glücksman, A. Studies on bone mechanics *in vitro*: II. The role of tension and pressure in chondrogenesis. *J. Anat.* 73:39–55, 1939.

[17]Hancox, N. M. Biology of Bone. Cambridge University Press, 1972.

[18]Iannacone, W., E. Korostoff, and S. R. Pollack. Microelectrode study of stress-generated potentials obtained from uniform and nonuniform compression of human bone. *J. Biomed. Mater. Res.* 13:753–763, 1979.

[19]Jacobs, C. R., C. E. Yellowley, B. R. Davis, Z. Zhou, J. M. Cimbala, and H. J. Donahue. Differential effect of steady versus oscillating flow on bone cells. *J. Biomech.* 31:969–976, 1998.

[20]Katz, J. L. Anisotropy of Young's modulus of bone. *Nature* 283:106–107, 1980.

[21]Katz, J. L. Hard tissue as a composite material. I. Bounds on the elastic behavior. *J. Biomech.* 4:455–473, 1971.

[22]Knothe Tate, M. L. Whither flows the fluid in bone? An osteocyte's perspective. *J. Biomech.* 36:1409–1424, 2003.

[23]Lakes, R. S. Materials with structural hierarchy. *Nature* 361:511–515, 1993.

[24]Lakes, R. S. Viscoelastic properties of cortical bone. In: Bone Mechanics Handbook, 2nd ed., edited by S. C. Cowin. Boca Raton, FL: CRC Press, 2001.

[25]Lakes, R. S. Viscoelastic Solids. Boca Raton, FL: CRC Press, 1998.

[26]Martin, R. B., and D. B. Burr. Structure, Function and Adaptation of Compact Bone. Raven Press, 1989.

[27]McCreadie, B. R., and S. J. Hollister. Strain concentrations surrounding an ellipsoid model of lacunae and osteocytes. *CMBBE* 1:61–68, 1997.

[28]McLean, F. C., and M. R. Urist. Bone: Fundamentals of the Physiology of Skeletal Tissue, 3rd ed. Chicago, IL: The University of Chicago Press, 1968.

[29]Murdoch, P., S. Benzley, T. Blacker, and S. A. Mitchell. The spatial twist continuum: A connectivity based method for representing all-hexahedral finite element meshes. *Finite Elem Anal. Des.* 28:137–149, 1997.

[30]Petrov, N., S. Pollack, and R. Blagoeva. A discrete model for streaming potentials in a single osteon. *J. Biomech.* 22(6–7):517–521, 1989.

[31]Piekarski, K., and M. Munro. Transport mechanism operating between blood supply and osteocytes in long bones. *Nature* 269:80–82, 1977.

[32]Qin, Y. X., K. J. McLeod, F. Guilak, F. P. Chiang, and C. T. Rubin. Correlation of bony ingrowth to the distribution of stress and strain parameters surrounding a porous-coated implant. *J. Orthop. Res.* 14:862–870, 1996.

[33]Rubin, C. T., and K. J. McLeod. Promotion of bony ingrowth by frequency-specific, low-amplitude mechanical strain. *Clin. Orthop.* 298:165–174, 1994.

[34]Rubin, C. T., and L. E. Lanyon. Limb mechanics as a function of speed and gait: A study of functional strains in the radius and tibia of horse and dog. *J. Exp. Biol.* 110:187–211, 1982.

[35]Rubin, C. T., and L. E. Lanyon. Regulation of bone formation by applied dynamic loads. *J. Bone Jt. Surg. Am.* 66:397–402, 1984.

[36]Salzstein, R. A., and S. R. Pollack. Electromechanical potentials in cortical bone. II. Experimental analysis. *J. Biomech.* 20(1):271–280, 1987.

[37]Salzstein, R. A., S. R. Pollack, A. F. T. Mak, and N. Petrov. Electromechanical potentials in cortical bone. I. A continuum approach. *J. Biomech.* 20(1):261–270, 1987.

[38]Scheidegger, A. E. The Physics of Flow Through Porous Media. New York: MacMillan, 1957.

[39]Starkebaum, W., S. R. Pollack, and E. Korostoff. Microelectrode studies of stress-generated potentials in four-point bending of bone. *J. Biomed. Mater. Res.* 13:729–751, 1979.

[40]Swan, C. C. http://www.engineering.uiowa.edu/~swan/software/fendac.pdf. FENDAC User's Manual. 2003.

[41]Swan, C. C. Techniques for stress- and strain-controlled homogenization of inelastic periodic composites. *Comput. Meth. Appl. Mfech. Eng.* 117:249–267, 1994.

[42]Swan, C. C., R. S. Lakes, R. A. Brand, and K. J. Stewart. Micromechanically based poroelastic modeling of fluid flow in Haversian bone. *J. Biomech. Eng.* 125:25–37, 2003.

[43]Tsay, R.-Y., and S. Weinbaum. Viscous flow in a channel with periodic crossbridging fibers: Exact solutions and Brinkman approximation. *J. Fluid Mech.* 226:125–148, 1991.

[44]Wang, L., S. C. Cowin, S. Weinbaum, and S. P. Fritton. Modeling tracer transport in an osteons under cyclic loading. *Ann. Biomed. Eng.* 28:1200–1208, 2000.

[45]Weinbaum, S., S. C. Cowin, and Y. Zeng. A model for the excitation of osteocytes by mechanical loading-induced bone fluid shear stresses. *J. Biomech.* 27:339–360, 1994.

[46]You, L., S. C. Cowin, M. B. Schaffler, and S. Weinbaum. A model for strain amplification in the actin cytoskeleton of osteocytes due to fluid drag on the pericellular matrix. *J. Biomech.* 34:1375–1386, 2001.

[47]Zhang, D., S. Weinbaum, and S. C. Cowin. Estimates of the peak pressures in bone pore water. *J. Biomech. Eng.* 120:697–703, 1998.

[48]Zhang, D., S. Weinbaum, and S. C. Cowin. On the calculation of bone pore water pressure due to mechanical loading. *Int. J. Solids Struct.* 35:4981–4997, 1998.